

Tuning two-dimensional electron and hole gases at $\text{LaInO}_3/\text{BaSnO}_3$ interfaces by polar distortions, termination, and thickness

Wahib Aggoune^{1,*} and Claudia Draxl^{1,2}

¹*Institut für Physik und IRIS Adlershof, Humboldt-Universität zu Berlin, 12489 Berlin, Germany*

²*European Theoretical Spectroscopy Facility (ETSF)*

(Dated: January 24, 2022)

Two-dimensional electron gases (2DEG), arising due to quantum confinement at interfaces between transparent conducting oxides, have received tremendous attention in view of electronic applications. Here, we explore the potential of interfaces formed by two lattice-matched wide-gap oxides of emerging interest, *i.e.*, the polar, orthorhombic perovskite LaInO_3 and the non-polar, cubic perovskite BaSnO_3 , employing first-principles approaches. We find that the polar discontinuity at the interface is mainly compensated by electronic relaxation through charge transfer from the LaInO_3 to the BaSnO_3 side. This leads to the formation of a 2DEG hosted by the highly-dispersive Sn-*s*-derived conduction band and a 2D hole gas of O-*p* character, strongly localized inside LaInO_3 . We rationalize how polar distortions, termination, thickness, and dimensionality of the system (periodic or non-periodic) can be exploited in view of tailoring the 2DEG characteristics, and why this material is superior to the most studied prototype $\text{LaAlO}_3/\text{SrTiO}_3$.

INTRODUCTION

Heterostructures of transparent conducting oxides (TCOs) have attracted the attention of researchers in view of both fundamental research as well as potential applications [1, 2]. Among them, interfaces of the perovskite materials LaAlO_3 and SrTiO_3 are most studied prototypes due to the emergence of fascinating physical phenomena including superconductivity, ferromagnetism [3], and interfacial two-dimensional electron gases (2DEG) [1]. The latter is mainly a consequence of the electronic reconstruction to compensate the interfacial polar discontinuity induced by deposition of the polar material LaAlO_3 formed by alternatingly charged $(\text{LaO})^+$ and $(\text{AlO}_2)^-$ planes on a neutral, TiO_2 -terminated SrTiO_3 substrate. The 2DEG density confined within the SrTiO_3 side of the interface can reach 0.5 electrons (e) per a^2 (a being the lattice parameter of SrTiO_3), corresponding to $\sim 3.3 \times 10^{14} \text{cm}^{-2}$ for a complete compensation of the formal polarization induced within LaAlO_3 [4]. However, in real samples, the presence of defects impact both, polar discontinuity and electronic reconstruction, and thus carrier mobilities [5]. This includes cation intermixing [5, 6], oxygen vacancies [7], edge dislocations [8], and changes in surface stoichiometry [9]. Overall, the electron mobilities at such an interface are very sensitive to growth conditions [5]. Besides these extrinsic effects, the low interfacial mobility of this material system is also caused by the low-dispersion (large effective electron masses) of the partially occupied Ti-*d* states. Further, scattering of electrons within these bands induced by significant electron-phonon coupling (EPC) decreases the mobility from $10^4 \text{cm}^2\text{V}^{-1}\text{s}^{-1}$ at low temperature, to $1 \text{cm}^2\text{V}^{-1}\text{s}^{-1}$ at room temperature [1, 10].

According to the polar-catastrophe model, in a perfect $\text{LaAlO}_3/\text{SrTiO}_3$ interface, the formal polarization (P_{LAO}^0) allows for an insulator-to-metal transition at the interface beyond a certain thickness (t_c) of LaAlO_3 . Estimating this quantity by considering the energy difference between the valence-band edge of LaAlO_3 and the conduction-band edge of SrTiO_3 [4, 11], one obtains a value of 3.5 unit cells. Higher t_c values reported theoretically and experimentally, are due to structural relaxations, *i.e.*, polar distortions that induce a polarization opposite to P_{LAO}^0 . Such polar distortions that are not considered in the polar-catastrophe model, maintain the insulating character of the interface above 3.5 unit cells as confirmed theoretically [2, 13] and later observed experimentally [14]. These distortions appear mainly in the LaAlO_3 side of the interface and arise due to changes inter-plane distances between La and Al planes upon interface formation. More recently, a competition between polar and nonpolar distortions through octahedra tilts has been observed [5]. Interestingly, the dependence of the octahedra tilts on the LaAlO_3 thickness can be exploited to tune the functionality of such interface [5]. We expect fascinating characteristics to occur when involving a polar material with pristine octahedral distortions such as a perovskite with an orthorhombic primitive cell.

Focusing first on nonpolar candidates as the substrate, cubic BaSnO_3 (BSO) has emerged as a most attractive system to overcome the limitations of SrTiO_3 , as it exhibits extraordinary room-temperature mobilities, reaching $320 \text{cm}^2\text{V}^{-1}\text{s}^{-1}$ [16–21]. This value is the highest ever measured in a TCO and attributed to the low effective electron mass as well as to the long relaxation time of the longitudinal optical phonon scattering compared to SrTiO_3 [16, 22, 23]. In contrast to other suggested polar materials to be combined with BaSnO_3 , such as LaScO_3 [17], LaGaO_3 [18], or LaAlO_3 [24], LaInO_3 (LIO) has the advantage of being nearly lattice matched to BaSnO_3 and exhibiting a favorable band offset to con-

* aggoune@physik.hu-berlin.de

fine a 2DEG within the BaSnO₃ side [1, 19–21, 25]. Interestingly, it has an orthorhombic structure with tilted InO₆ octahedra, thus ideal for exploring also interfaces made of tilted and nontilted components.

In a previous work [27], it was shown by transmission electron microscopy (TEM) that LaInO₃ can be coherently grown on (001) BaSnO₃, forming a sharp interface with negligible atomic disorder or misfit dislocations. This characteristic makes such an interface fascinating, since—as reported for LaAlO₃/SrTiO₃ [8]—the interface conductivity and the mobility of the electron gas are enhanced by minimizing the dislocation density. Later it was shown by HRTEM analysis [8] that even if the BaO termination of the (001) BaSnO₃ surface is most favorable, the LaInO₃/BaSnO₃ interface (termed LIO/BSO from now on) is characterized by the LaO/SnO₂ termination, which is key for the formation of a 2DEG. Thereby, cation intermixing at the interface was rated to be negligible. Therefore, the combination of LaInO₃ and BaSnO₃ exhibits all the key features and appears superior to LaAlO₃/SrTiO₃ interfaces for reaching a high mobility 2DEG.

In this work, we explore the characteristics of ideal LIO/BSO interfaces, based on density-functional-theory (DFT), also employing many-body perturbation theory where needed. We focus only on intrinsic effects that may play a role in compensating the interfacial polar discontinuity, *i.e.*, electronic reconstruction (formation of 2DEG) and possible structural distortions (formation of a depolarization field). Considering first periodic heterostructures, we address the competition between the polar distortions and the 2DEG charge density to compensate the interfacial polar discontinuity, upon increasing the thickness of the polar LaInO₃ block. Second, we discuss the impact of the interface termination that may give rise to either a 2DEG or 2D hole gas (2DHG). Finally, motivated by the advancements in synthesis techniques and in control of nanoscale structures [29], we provide a detailed comparison between the characteristics of the 2DEG in a periodic heterostructure and a non-periodic LIO/BSO interface, discussing how one can exploit dimensionality for tailoring the properties of the 2DEG. Overall, our results demonstrate the potential of this material combination for tuning and achieving high electron density and mobility.

RESULTS AND DISCUSSION

Pristine materials

Before discussing the results for the periodic heterostructures LIO/BSO, we summarize the basic properties of the pristine materials. BaSnO₃ crystallizes in the cubic space group Pm $\bar{3}$ m and is built by alternating neutral (BaO)⁰ and (SnO₂)⁰ planes along the cartesian directions, making it a nonpolar material. Its static dielectric constant was estimated to be about 20 [16]. The calculated lattice constant of 4.119 Å obtained with the

PBEsol functional is in excellent agreement with experiment [16]. LaInO₃ has an orthorhombic perovskite structure of space group Pbnm, containing four formula units per unit cell. The optimized structural parameters $a=5.70$ Å, $b=5.94$ Å, and $c=8.21$ Å are in good agreement with experimental values [30]. The corresponding pseudocubic unit cell is defined such to have the same volume per LaInO₃ formula as the orthorhombic structure [for more details, we refer to the Supporting Information (SI) [31]]. Its calculated lattice parameter is about 4.116 Å. In LaInO₃, the InO₆ octahedra are tilted along the pseudocubic unit cell directions with an $a^-a^-c^+$ pattern according to the Glazer notation [32]. Considering the formal ionic charges of La (+3), In (+3), and O (-2), the charged (LaO)⁺¹ and (InO₂)⁻¹ planes along the pseudocubic unit cell [100], [010], and [001] directions make LaInO₃ a polar material (see supplementary figure 1).

The calculated lattice mismatch between the cubic BaSnO₃ and the pseudocubic LaInO₃ unit cells is about 0.07%, suggesting a coherent interface as confirmed experimentally [27]. In the latter work, it was shown that LaInO₃ can be favorably grown on top of a (001) BaSnO₃ substrate along the three pseudocubic unit cell directions, preserving the polar discontinuity at the interface, regardless of the orientation. Here, we consider the interface formed by [001]-oriented LaInO₃ (*i.e.*, $c=8.21$ Å corresponds to the out-of-plane direction) on top of the (001) BaSnO₃ surface (see supplementary figure 1).

The electronic properties of both bulk BaSnO₃ and LaInO₃ have been reported by us in previous works [7, 9], revealing PBEsol band gaps of 0.9 and 2.87 eV, and quasiparticle band gaps of 3.5 and 5.0 eV, respectively, as obtained by the G_0W_0 correction to results obtained by the exchange-correlation functional HSE06 ($G_0W_0@HSE06$). In both cases, the valence-band maximum is dominated by O- p states, while, the conduction-band minimum has Sn- s and In- s character, respectively.

Stoichiometric periodic heterostructures

In Fig. 1 we show a comprehensive compilation of the electronic properties of the LIO/BSO interface in a periodic heterostructure. Thereby, n-type (LaO/SnO₂) and p-type (InO₂/BaO) building blocks are periodically replicated in the out-of-plane direction (z). In this case, the system is stoichiometric and ideally suited for investigating the electronic reconstruction due to the polar discontinuity. The BaSnO₃ block has a thickness of 10 unit cells which is enough to minimize the interaction with its replica. It is determined by making sure that the central part of the BaSnO₃ block behaves like in its bulk counterpart (see supplementary figure 2). The LaInO₃ block has a thickness of 12 pseudocubic unit cells. (We use the notation LIO₁₂/BSO₁₀ heterostructure in the following). Since the LaInO₃ block has different terminations on the two sides, a formal polarization of $P_0 = e/2a^2=0.47$ C m⁻², oriented from the (InO₂)⁻¹ to the (LaO)⁺¹ plane,

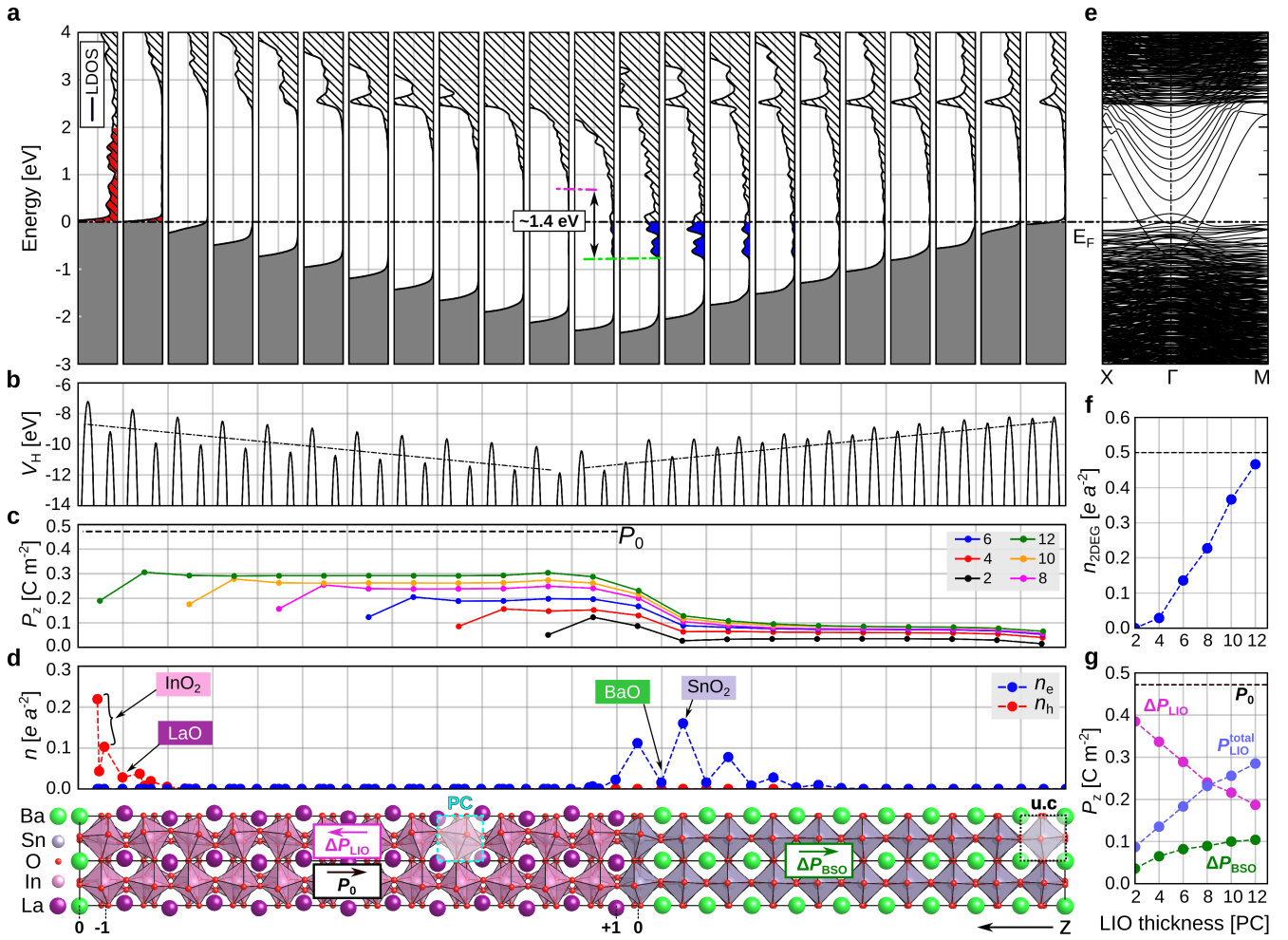


FIG. 1. Stoichiometric periodic heterostructure: the system is formed by $\text{LiO}_{12}/\text{BSO}_{10}$ in out-of-plane direction z (bottom), that is shared between panels (a), (b), (c), and (d) as their horizontal axis. P_0 is the formal polarization oriented from the $(\text{InO}_2)^{-1}$ to the $(\text{LaO})^{+1}$ plane. (a) Local density of states per unit cell (LDOS) where the Fermi level is set to zero (also in panel (e)). The shaded gray area indicates the occupied valence band. The partially unoccupied valence (hole) and the occupied conduction (electron) states, resulting from electronic reconstruction, are highlighted by red and blue color, respectively. The dashed green and pink lines indicate the alignment of the conduction-band edges of BaSnO_3 and LaInO_3 at the interface. (b) In-plane averaged electrostatic potential along the z direction. The dashed lines are guides to the eye, highlighting the trend of the potential. (c) Total polarization per unit cell computed for different LaInO_3 thicknesses (in units of the pseudocubic unit cell, PC). (d) Distribution of the electron (hole) charge densities obtained by integrating over the occupied conduction (unoccupied valence) states shown with blue (red) colored area in panel (a). (e) Electronic band structure along X- Γ -M. (f) Density of the 2DEG in electrons per BaSnO_3 surface unit cell (e per \AA^2). (g) Total polarization ($P_{\text{total}}^{\text{LIO}}$, violet) within the LaInO_3 block and changes of polar distortions within the LaInO_3 (ΔP_{LIO} , magenta) and BaSnO_3 (ΔP_{BSO} , green) side as a function of the LaInO_3 thickness. The respective orientations are shown in the structural model.

is induced (black arrow in the bottom panel of Fig. 1). As BaSnO_3 is a nonpolar material, this gives rise to a polar discontinuity at the interface.

The charge reconstruction is evident from the electronic band structure [Fig. 1(e)] showing that the combination of these two insulators has metallic character. From the local density of states (LDOS, per unit cell) depicted in panel (a) along the z direction, we can clearly see that the dipole induced within the LaInO_3 side causes an upward shift of the valence-band edge, evolving be-

tween the $(\text{LaO})^{+1}$ and $(\text{InO}_2)^{-1}$ terminations. This is also reflected in the in-plane averaged electrostatic potential shown in panel (b) (for more details see supplementary figure 9). At the latter termination, the valence-band maximum crosses the Fermi level inside LaInO_3 , leading to a charge transfer to the BaSnO_3 side in order to compensate the polar discontinuity. Consequently, the bottom of the conduction band of BaSnO_3 becomes partially occupied, giving rise to a 2DEG confined within three unit cells (~ 10 \AA). A 2DHG forms in the LaInO_3

side localized within one pseudocubic unit cell ($\sim 4 \text{ \AA}$). Integrating over these now partially occupied conduction states (see supplementary methods), we find that the 2DEG density reaches a value of $2.7 \times 10^{14} \text{ cm}^{-2}$ *i.e.*, $\sim 0.46 e$ per a^2 (a^2 being the unit cell area of bulk BaSnO_3). Obviously, the same value is obtained for the 2DHG when integrating over the now empty parts of the valence bands. The charge distribution shown in Fig. 1(d) reveals that the 2DEG is located mainly within the SnO_2 plane and exhibits Sn-*s* character. This highly-dispersive *s*-band suggests high mobility, unlike the situation in $\text{LaAlO}_3/\text{SrTiO}_3$. These results demonstrate the exciting potential of such a material combination as an ideal platform for achieving a high-density 2DEG. We also highlight the importance of the well-confined 2DHG hosted by O-*p* states in view of p-type conductivity. We note that in $\text{SrTiO}_3/\text{LaAlO}_3/\text{SrTiO}_3$, another heterostructures [35] formed by a polar and a nonpolar material, only recently the presence of a 2DHG has been confirmed experimentally [29]. The coexistence of high-density well-confined electron and hole gases within one system as shown here, appears as a promising platform for exploring also intriguing phenomena such as long-lifetime bilayer excitons [36] or Bose-Einstein condensation [37].

Polar distortions in stoichiometric periodic heterostructures

The 2DEG density reached in the periodic heterostructure $\text{LIO}_{12}/\text{BSO}_{10}$, being slightly lower than $0.5 e$ per a^2 , indicates that polar distortions are involved to partially compensate for the polar discontinuity. Looking into its optimized geometry, we find that the tilt of the octahedra decreases gradually from the LaInO_3 to the BaSnO_3 side [see Fig. 1(bottom panel)]. Consequently, the out-of-plane lattice spacing increases close to the interface by about 3% (see supplementary figure 2), in good agreement with an experimental observation [1]. We also find that the out-of-plane displacements of the inequivalent O atoms are not the same within all octahedra (see supplementary figure 2 and 3). Moreover, the distances between AO and BO_2 planes (A= Ba, La and B= Sn, In) across the interface are also unequal (see supplementary figure 2). Using a simple linear approximation for the local polarization based on Born effective charges (Z^*) [3, 6] of the atomic species (calculated for the pristine materials), we obtain a qualitative trend of the out-of-plane polarization induced by such structural distortions (see supplementary discussion). We note that due to the tilt of the octahedra, calculating the polarization for such a heterostructure is less straightforward than for, *e.g.*, $\text{LaAlO}_3/\text{SrTiO}_3$. We find that the structural distortions within the LaInO_3 side induce a polarization ΔP_{LIO} that counteracts the formal polarization P_0 . Moreover, the polar discontinuity at the interface is reduced by structural distortions within the BaSnO_3 side, inducing ΔP_{BSO} that is parallel to P_0 . The total polarization within the LaInO_3 side, $P_{\text{total}}^{\text{LIO}}$, shown in Fig. 1(g)

is the sum of $-\Delta P_{\text{LIO}}$ and P_0 . As expected for the particular case of $\text{LIO}_{12}/\text{BSO}_{10}$, the average polarization within LaInO_3 ($P_{\text{total}}^{\text{LIO}}$) is smaller than P_0 due to partial compensation by structural distortions. For this reason, the 2DEG density mentioned above is smaller than $0.5 e$ per a^2 . For better grasping the polar discontinuity at the interface, we plot the total polarization along the z direction [see Fig. 1(c)]. Focusing first on the particular case of $\text{LIO}_{12}/\text{BSO}_{10}$, we can clearly see that within the LaInO_3 side, it is smaller than P_0 and also non-negligible inside BaSnO_3 , making the polar discontinuity at the interface less pronounced. As we provide only a qualitative analysis of the polarization, we do not expect a full match between the values of the 2DEG and the corresponding polarization discontinuity. However, the obtained trend of the polarization strength is valuable to understand and explain the relationship between the calculated 2DEG density and the LaInO_3 thickness.

Impact of the LaInO_3 thickness in stoichiometric periodic heterostructures

Now, we fix the thickness of the BaSnO_3 building block to 10 unit cells and vary that of LaInO_3 between 2 and 12 pseudocubic unit cells, labeling the systems $\text{LIO}_m/\text{BSO}_{10}$ ($m=2, 4, 6, 8, 10, 12$). Before discussing the results, we note that the *critical* thickness, t_c , for an insulator-to-metal transition at the interface is about one pseudocubic LaInO_3 unit cell, when ignoring effects from structural relaxation as given by the polar catastrophe model [4, 11]. This value is obtained as $t_c = \epsilon_0 \epsilon_{\text{LIO}} \Delta E / e P_{\text{LIO}}^0$. Here, $\epsilon_{\text{LIO}} \sim 24$ is the relative static dielectric constant of LaInO_3 [30, 40], and $\Delta E = 1 \text{ eV}$ represents the energy difference between the valence-band edge of LaInO_3 and the conduction-band edge of BaSnO_3 at the interface, obtained by the PBEsol functional [see Fig. 1(a)]. In contrast to the *unrelaxed* $\text{LIO}_2/\text{BSO}_{10}$ system, where we find metallic character, with full electronic reconstruction of $0.5 e$ per a^2 (see supplementary figure 4), atomic relaxations lead to semiconducting character, *i.e.*, no formation of a 2DEG [see Fig. 1(f)]. We observe that the polar distortions that counteract the formal polarization P_0 , hamper the electronic reconstruction at the interface and, thus, the formation of a 2DEG, up to a *critical* thickness of 4 pseudocubic LaInO_3 unit cells [see Fig. 1(f)]. This result highlights the importance of structural relaxations for compensating the polar discontinuity and stabilizing the interface.

Focusing on the electronic charge, we find that at a thickness of 4 pseudocubic LaInO_3 unit cells, the density of the 2DEG is only about $0.03 e$ per a^2 [see Fig. 1(f)], *i.e.*, distinctively smaller than the nominal value of $0.5 e$ per a^2 . Increasing the LaInO_3 thickness, the 2DEG density increases progressively and reaches a value of $\sim 0.46 e$ per a^2 with 12 pseudocubic LaInO_3 unit cells. This means that the polar distortions are also non-negligible beyond the *critical* thickness. In Fig 1(g), we display the

averages of ΔP_{LIO} and ΔP_{total} for the considered structures $\text{LIO}_m/\text{BSO}_{10}$, finding that the polar distortions (total polarization) is maximal (minimal) at two pseudocubic LaInO_3 unit cells and decreases (increases) with LaInO_3 thickness. ΔP_{BSO} increases with LaInO_3 thickness, but it is smaller than its counterpart in LaInO_3 . As a result, the polar discontinuity at the interface increases with increasing LaInO_3 thickness [see Fig. 1(c)]. Hence, the 2DEG density increases accordingly in order to compensate it [see Fig. 1(f)].

For a more reliable estimation of the *critical* thickness of LaInO_3 for an insulator-to-metal transition, we evaluate ΔE by considering the quasiparticle band gaps of the constituents [7, 9]. Applying a scissor shift to the PBEsol band offset leads to a quasiparticle value of $\Delta E=3.4$ eV, in agreement with the band offset reported in Ref. [20] (see supplementary discussion). Thus, we obtain a $t_c=4$ pseudocubic LaInO_3 unit cell which is increased by 3 pseudocubic unit cells compared to that given by PBEsol offset (one pseudocubic unit cell). For the relaxed structures, we estimate t_c to be about seven pseudocubic LaInO_3 unit cells when considering quasiparticle band gaps, which is distinctively larger than the 4 pseudocubic unit cells derived from PBEsol [see Fig. 1(f)]. This result indicates that a thick LaInO_3 component is needed to reach high 2DEG densities in periodic heterostructures, as both sides contribute to the compensation of the polar discontinuity through atomic distortions. This result is inline with a previous theoretical discussion reported for oxide interfaces [13].

Proceeding now to the nature of the atomic distortions, we find that, in contrast to the $\text{LaAlO}_3/\text{SrTiO}_3$ interface where the unequal distances between La and Al planes dominate [14], the unequal displacements of the inequivalent oxygen atoms are most decisive for the polar distortions in the LaInO_3 side of the interface (see supplementary figure 2). This behavior is governed by the gradual tilts of octahedra across the interface which facilitates the compensation of the polar discontinuity. This indicates that below the *critical* thickness, this compensation happens through such atomic distortions, rather than elimination by ionic intermixing or other defects, explaining the sharp interface and negligible intermixing observed experimentally [27]. The latter characteristic is crucial for achieving a high-density 2DEG beyond t_c . The band offset at the interface shows that the conduction-band minimum of BaSnO_3 is about 1.4 eV below that of LaInO_3 , confining the 2DEG at the BaSnO_3 side [see Fig. 1(a)].

Non-stoichiometric n-type periodic heterostructure

Adopting thicker polar building blocks, *i.e.*, above 12 pseudocubic unit cells, the interaction between the n-type and the p-type interfaces is prevented. Due to the considerable computational costs, several models were proposed to predict the characteristics of such situation in oxide interfaces [13]. One of them is to consider non-stoichiometric structures, where the polar LaInO_3 block

is terminated by a $(\text{LaO})^{+1}$ plane on both sides. In this case, termed nn-type periodic heterostructure, the system is self-doped as the additional $(\text{LaO})^{+1}$ layer serves donor. As the LaInO_3 building block is symmetric, the formal polarization P_0 is induced from the middle of the slab outwards on both sides, that compensate each other. In this way, the built-in potential inside the LaInO_3 is avoided, while the discontinuity at the LIO/BSO interface is preserved. To this end, we consider a periodic heterostructure formed by 10 BaSnO_3 unit cells and 10 pseudocubic LaInO_3 unit cells, which is large enough to minimize the interaction between the periodic n-type interfaces [see Fig. 2(bottom) and supplementary figure 6].

The electronic band structure, obtained by PBEsol, shows that this system has metallic character, where the partial occupation of the conduction band amounts to 1 e per a^2 [see Fig. 2(e)]. The corresponding effective electron mass, being 0.24 m_e , is quite low compared with that of $\text{LaAlO}_3/\text{SrTiO}_3$ interfaces (0.38 m_e [35]), and suggests a high electron mobility. This value is close to that found for pristine BaSnO_3 (0.17 m_e obtained by PBEsol, 0.2 m_e by G_0W_0) [9]. In pristine SrTiO_3 , a transition from band-like conduction (scattering of renormalized quasiparticles) to a regime governed by incoherent contributions due to the interaction between the electrons and their phonon cloud has been reported upon increasing temperature [41]. In BaSnO_3 , the relaxation time for the longitudinal optical phonon scattering is found to be larger compared to SrTiO_3 , contributing to the high-room temperature mobility reported for the La-doped BaSnO_3 single crystals [23]. Based on this, a high room-temperature mobility is also expected at the here investigated interfaces as this material combination basically preserves the structure of the pristine BaSnO_3 [42]. Overall, significant polaronic effects are not expected. In both constituents, we find typical EPC effects on the electronic properties [7, 9], *i.e.*, a moderate renormalization of the band gap by zero point vibrations and temperature. Given the excellent agreement between theory and experiment that can explain all features of the optical spectra [7, 9], we conclude that polaronic distortions do not play a significant role. Thus, we do not expect a dramatically different behavior at the interfaces.

Before analyzing the spatial charge distribution, we note that in a pristine symmetric LaInO_3 slab, the electronic charge accumulates on its surfaces, accompanied by structural distortions that tend to screen the discontinuity of the polarization. Combined with BaSnO_3 , the polar distortions vanish at the LaInO_3 side but appear in the BaSnO_3 building block and are accompanied by a charge redistribution [see Fig. 2(a) and (c)]. In Fig. 2(c), we display the polarization induced by the structural distortions along the slab. We find that the gradual decrease of the octahedra tilt from the LaInO_3 to the BaSnO_3 side enlarges the out-of-plane lattice spacing at the interface and enhances the unequal oxygen-cation displacements within the BaSnO_3 side (see supplementary figure 6). This, in turn, induces a gradually decreasing polariza-

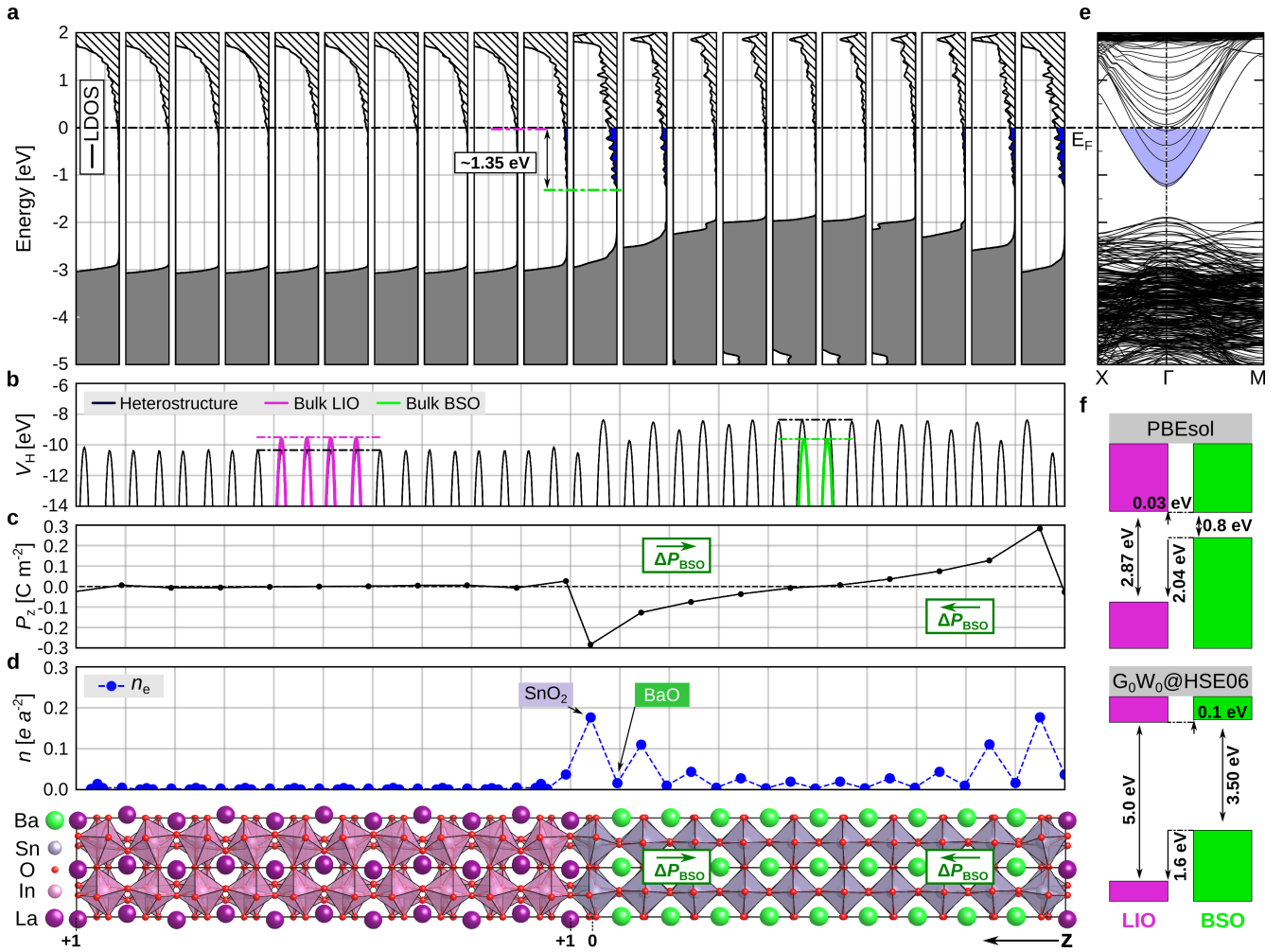


FIG. 2. Non-stoichiometric periodic nn-type heterostructure: the system is formed by $\text{LIO}_{10}/\text{BSO}_{10}$ in out-of-plane direction z (bottom), that is shared between panels (a), (b), (c), and (d) as their horizontal axis. The LaInO_3 block is terminated by a $(\text{LaO})^{+1}$ plane on both sides. (a) Local density of states per unit cell (LDOS). The Fermi level is set to zero, and the electron population of the (original) conduction bands is shown as shaded blue area (also in panel (e)). The dashed green and pink lines indicate the alignment of the conduction-band edges of the two materials at the interface. (b) In-plane averaged electrostatic potential along the z direction. (c) Total polarization per unit cell. (d) Distribution of the electron charge density obtained by integrating over the occupied conduction states indicated by the blue area in panel (a). (e) Electronic band structure along X- Γ -M. (f) Band alignment as obtained by using the band gaps of the bulk systems (PBEsol [top] and G_0W_0 @HSE06 [bottom]), considering the energy difference between the potential of the bulk and the periodic heterostructure as shown in panel (b). The alignment at the interface obtained by PBEsol can be seen in panel (a).

tion (ΔP_{BSO}) oriented away from the interface. Due to this local dipole, the BaSnO_3 conduction-band edge is shifted downwards near the interface, leading to partial charge redistribution [see Fig. 2(a) and (d)], and being also evident in the in-plane averaged electrostatic potential [panel (b)]. Integrating the LDOS over the partially occupied conduction states, we find that the 2DEG is confined within three unit cells, amounting to $0.5 e$ per a^2 at each side [see Fig. 2(d)]. Thereby the 2DEG is mainly hosted by Sn- s states within the SnO_2 planes. The valence and conduction-band edges at the LaInO_3 side are almost the same in all pseudocubic unit cells as the polar distortions are negligible (only nonpolar tilts)

[see Figs. 2(a) and (c)]. These results are inline with the trend of the polarization and the 2DEG density obtained for the stoichiometric periodic system. While in the latter, we observed decreasing (increasing) structural distortions in the LaInO_3 (BaSnO_3) side as a function of LaInO_3 thickness [see Fig. 1(g)], here, the polar distortions vanish (are enhanced) at the LaInO_3 (BaSnO_3) side of the interface. Consequently, the conduction-band minimum of the BaSnO_3 side is lowered by about 1.35 eV with respect to that of LaInO_3 [see Fig. 2(a)]. This value is also inline with that estimated for the stoichiometric periodic heterostructure $\text{LIO}_{12}/\text{BSO}_{10}$ (~ 1.4 eV). Such an offset is crucial for confining the 2DEG in order to

reach a value of $0.5 e$ per a^2 [see Fig. 2(a) and (d)].

Note that here, we can determine the band offsets by considering the respective quasiparticle gaps of the pristine materials [7, 9] as well as an alternative approach based on the electrostatic potential [10] (see Fig. 2(b) and supplementary discussion). We find that, the conduction-band offset between the middle of the BaSnO_3 and LaInO_3 blocks is almost the same when using quasiparticle or PBEsol band gaps [see Fig. 2(b) and (f)]. Thus, we conclude that PBEsol is good enough to capture band offset and charge distribution at the interface. The latter conclusions are confirmed by calculations using HSE06 for a smaller (feasible) nn-type system (see supplementary figure 7).

Non-stoichiometric pp-type periodic heterostructure

Calculations for a periodic pp-type heterostructure (see supplementary figure 5) with $(\text{InO}_2)^{-1}$ termination on both sides of LaInO_3 reveal a 2DHG with a density of $0.5 e$ per a^2 . Interestingly, the hole stays at the LaInO_3 side, confined within one pseudocubic unit cell. Like in the periodic nn-type heterostructure, the tilt of the octahedra decreases gradually from the LaInO_3 to BaSnO_3 side. However, the BaO termination in the pp-type case favors nonpolar distortions within the BaSnO_3 side, *i.e.*, equal displacements of the inequivalent O atoms, while polar distortions appear only in the LaInO_3 side. Consequently, local dipoles are induced in the latter, pushing up its valence-band edge above that of BaSnO_3 (see supplementary figure 5). Hence, the 2DHG exhibiting O- p character, stays on the LaInO_3 side of the interface. It has been shown recently by a combined theoretical and experimental investigation [8] that the n-type interface is more favorable than the p-type interface. Since at the BaO -terminated p-type interface, the 2DHG stays within the LaInO_3 side it contributes less to the compensation of the interfacial polar discontinuity. In contrast, the SnO_2 -terminated n-type interface allows for electronic charge transfer to the BaSnO_3 side, forming a 2DEG that compensates the interfacial polar discontinuity more efficiently (see supplementary discussion).

Stoichiometric non-periodic interface

Now, we investigate the case of a non-periodic LIO/BSO interface, consisting of a thin LaInO_3 layer on top of a (001) BaSnO_3 substrate. Considering stoichiometric systems, we only focus on the n-type interface as it is predicted to be more favorable [8]. For BaSnO_3 , we find that 11 unit cells are enough to capture the extension of the structural deformations and the 2DEG distribution away from the interface. We then vary the thickness of LaInO_3 between one and eight pseudocubic unit cells, labeling the systems as $\text{LIO}_n/\text{BSO}_{11}$ ($n=1, 2, 4, 6, 8$). In Fig. (bottom panel), we show the optimized geometry of $\text{LIO}_8/\text{BSO}_{11}$. The BaSnO_3 substrate terminates with a $(\text{SnO}_2)^0$ plane at the interface, and the surface termination of LaInO_3 is a $(\text{InO}_2)^{-1}$ plane. Thus,

LaInO_3 is stoichiometric and has a formal polarization of $P_0=0.47 \text{ C m}^{-2}$, oriented from the surface to the interface, as in the stoichiometric periodic heterostructures discussed above.

Electronic reconstruction, that leads to a metallic character, is evident from the resulting band structure, where the valence and conduction bands overlap at the Γ point [see Fig. (e)]. In the LDOS, we clearly see that the dipole induced within LaInO_3 causes an upward shift of the valence-band edge (most pronounced at the surface) which is also evident in the in-plane averaged electrostatic potential [see Figs. (a) and (b)]. At the surface, the valence-band edge crosses the Fermi level, leading to a charge transfer across the interface that counteracts the polar discontinuity [see Fig. (a)]. Consequently, the bottom of the conduction band becomes partially occupied within the BaSnO_3 side, giving rise to a 2DEG that is confined within five unit cells ($\sim 20 \text{ \AA}$) [see Fig. (d)]. The 2DHG formed at the surface is localized within one pseudocubic LaInO_3 unit cell ($\sim 4 \text{ \AA}$). In this case, the conduction-band minimum of the BaSnO_3 building block is about 1.7 eV below that of LaInO_3 [Fig. 1(a)], in agreement with an experimental observation of 1.6 eV [20]. Integrating the LDOS over the region of these partially filled states, we find that the 2DEG density (and likewise the 2DHG density) reaches a value of $2.9 \times 10^{14} \text{ cm}^{-2}$ *i.e.*, $\sim 0.49 e$ per a^2 .

By increasing the LaInO_3 thickness from one to eight pseudocubic unit cells, the polar distortions (ΔP_{LIO}) decrease, being accompanied by an electronic charge transfer from the surface to the interface [see Fig. (f) and (g)]. Compared to the periodic heterostructure [Fig. 1(c)], they are less pronounced at the BaSnO_3 side [Fig. (c)]. This enhances the polar discontinuity (see supplementary figure 8) and thus, the 2DEG density that reaches a higher value than in the periodic systems with similar LaInO_3 thickness [see Fig. (f)]. Focusing on the charge confinement, the conduction-band edge in the BaSnO_3 side is gradually shifted up when moving away from the interface as ΔP_{BSO} is less pronounced. This allows an extension of the 2DEG up to five unit cells ($\sim 20 \text{ \AA}$) in the BaSnO_3 (substrate) compared to three unit cells in the periodic heterostructure case [see Fig. (d)]. The enhanced polar discontinuity reduces the *critical thickness* to only two pseudocubic LaInO_3 unit cells compared to four found for the periodic heterostructure, when relying on PBEsol [see Fig. (f)]. Based on the quasiparticle band gaps, however, we estimate t_c to be five pseudocubic LaInO_3 unit cells in the non-periodic system compared to seven in the periodic case. Overall tuning of the 2DEG charge density through the LaInO_3 thickness is possible, and remarkably, also the type of heterostructure (*i.e.*, periodic or non-periodic) impacts its spacial distribution. Both aspects can be exploited to tune the characteristic of the 2DEG.

In view of realistic applications, it is worth considering the results presented here in the context of existing experimental research on LIO/BSO interfaces. A

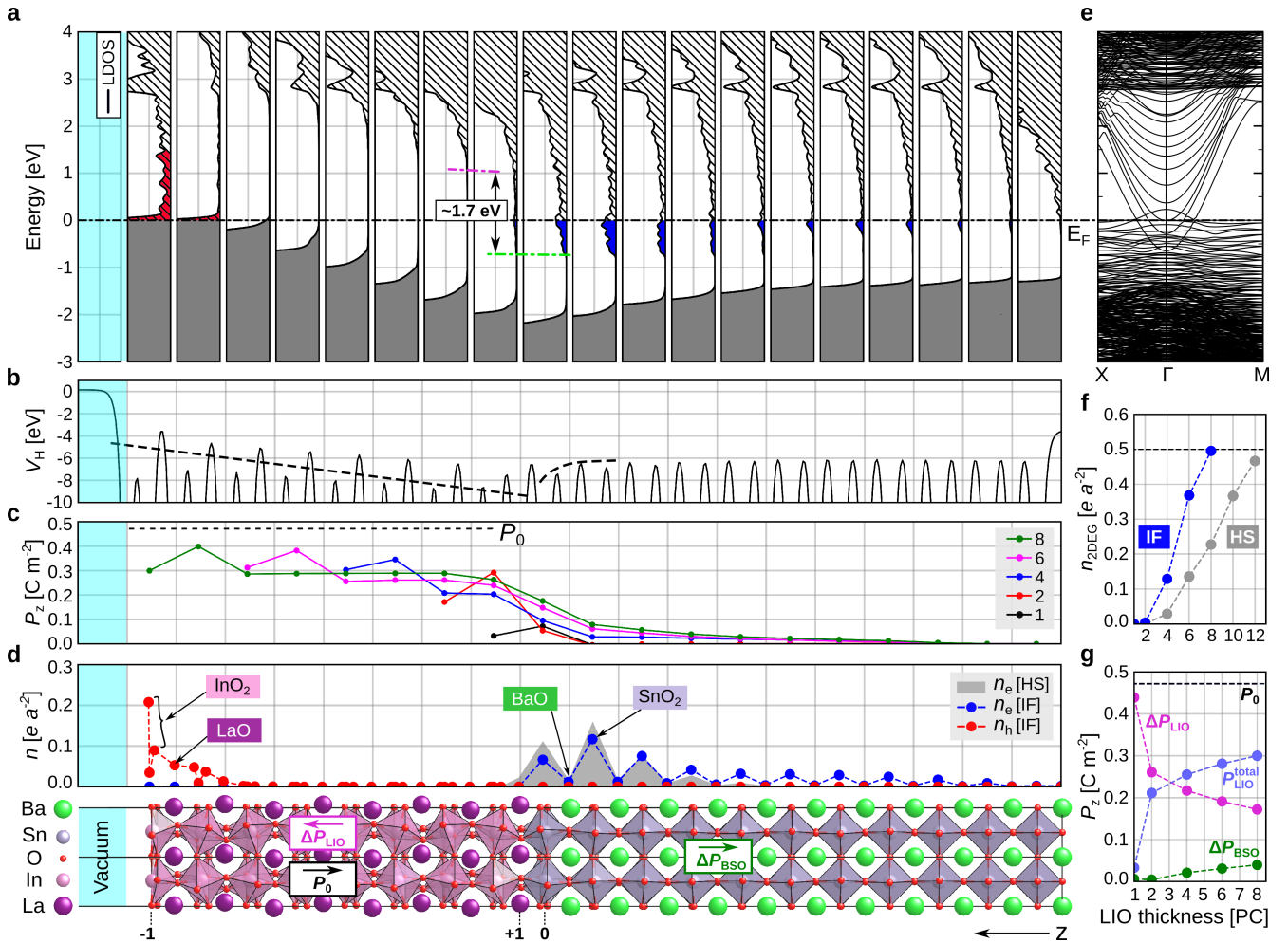


FIG. 3. Stoichiometric non-periodic interface (here termed IF): the system is formed by LIO₈/BSO₁₁ in out-of-plane direction z (bottom), that is shared between panels (a), (b), (c), and (d) as their horizontal axis. P_0 is the formal polarization oriented from the (InO₂)⁻¹ plane towards the (LaO)⁺¹ plane at the interface. (a) Local density of states per unit cell (LDOS) with the Fermi level being set to zero (also in panel (e)). The shaded gray area indicates the occupied valence states. The depleted valence band region (holes) and the occupied conduction band region (electrons) resulting from electronic reconstruction, are highlighted by red and blue color, respectively. The dashed green and pink lines indicate the alignment of the conduction-band edges of the two materials at the interface. (b) In-plane averaged electrostatic potential along the z direction. (c) Total polarization per unit cell computed for different LaInO₃ thicknesses (in units of the pseudocubic unit cell, PC). (d) Distribution of the electron (hole) charge densities obtained by integrating the LDOS indicated by blue (red) color in panel (a). For comparison, the 2DEG distribution in the periodic heterostructure LIO₁₂/BSO₁₀ (here termed HS) is shown by the shaded gray area. (e) Electronic band structure along X- Γ -M. (f) Density of the 2DEG in e per a^2 in the non-periodic (blue) and periodic (gray) heterostructures. (g) Total polarization (P_{total}^{LIO} , violet) within the LaInO₃ side and changes of polar distortions within LaInO₃ (ΔP_{LIO} , magenta) and BaSnO₃ (ΔP_{BSO} , green) side as a function of LaInO₃ thickness. The respective orientations are shown in the structural model.

main challenge here is the quality of the BaSnO₃ substrate [44]. Previous experimental works [1, 20] investigated a field effect transistor, formed by a LaInO₃ gate and a La-doped BaSnO₃ channel on a SrTiO₃ substrate. An enhancement of conductance with increasing LaInO₃ thickness was observed, but no indication of a *critical* thickness for an insulator-to-metal transition at the interface. A maximal 2DEG density of only 3×10^{13} ($0.05 e$ per a^2) was reported for 4 pseudocubic LaInO₃ unit cells, and a decrease beyond it. We assign the differences to

our predictions for non-periodic interfaces mainly to the high density of structural defects (*e.g.*, dislocations) due to the large mismatch ($\sim 5\%$) between the channel and the substrate. The La doping, needed to compensate the acceptors induced by such dislocations, may cause an alleviation of the polar discontinuity at the interface and, hence, limit the 2DEG density. On the other hand, it makes the system metallic without a clear *critical* thickness. With the recent advances in achieving high-quality BaSnO₃ and LaInO₃ single crystals [7, 30, 44] as well as

interfaces [8, 27], our predictions open up a perspective for exploring interfacial charge densities in combinations of these materials in view of potential electronic applications.

Conclusions

In summary, we have presented the potential of combining nonpolar BaSnO₃ and polar LaInO₃ for reaching a high interfacial carrier density. Our calculations show that, depending on the interface termination, both electron and hole gases can be formed that compensate the polar discontinuity. The gradual decrease of octahedra tilts from the orthorhombic LaInO₃ to the cubic BaSnO₃ side increases the out-of-plane lattice spacing at the interface and governs the unequal oxygen-cation displacements within the octahedra. The latter distortions induce a depolarization field, counteracting the formal polarization in the LaInO₃ block and hampering electronic reconstruction, *i.e.* the formation of a 2DEG at the interface up to a *critical* LaInO₃ thickness of seven (five) pseudocubic unit cells for periodic (non-periodic) heterostructures. While the PBEsol functional provides a good description of the interfacial charge-density distributions as well as the type of band offset, it fails to determine t_c reliably, as the knowledge of the quasiparticle gaps of the pristine materials is required. The polar distortions (polar discontinuity) decrease (increases) with LaInO₃ thickness, leading to a progressive charge transfer until reaching a 2DEG density of 0.5 e per surface unit cell. The electronic charge density is hosted by a highly dispersive Sn- s -derived conduction band, suggesting a high carrier mobility. Overall, the 2DEG charge density can be tuned through the LaInO₃ thickness. Interestingly, also the type of interface (*i.e.*, periodic or non-periodic heterostructure) strongly impacts its density and spatial confinement. All these effects can be exploited in view of tailoring the characteristics of the 2DEG.

METHODS

Theory

Ground-state properties are calculated using density-functional theory (DFT), within the generalized gradient approximation (GGA) in the PBEsol parameterization [45] for exchange-correlation effects. All calculations are performed using FHI-aims [46], an all-electron full-potential package, employing numerical atom-centered orbitals. For all atomic species we use a *tight* setting with a *tier 2* basis set for oxygen, *tier1+fg* for barium, *tier1+gpfd* for tin, *tier 1+hfdg* for lanthanum, and *tier 1+gpffhf* for indium. The convergence criteria are 10^{-6} electrons for the density, 10^{-6} eV for the total energy, 10^{-4} eV \AA^{-1} for the forces, and 10^{-4} eV for the eigenvalues. Lattice constants and internal coordinates are optimized for all systems until the residual forces on each atom are less than 0.001 eV \AA^{-1} . The sampling of the Brillouin zone is performed with an $8 \times 8 \times 8$ \mathbf{k} -grid for

bulk BaSnO₃ and a $6 \times 6 \times 4$ \mathbf{k} -grid for bulk LaInO₃. These parameters ensure converged total energies and lattice constants of 8 meV per atom and 0.001 \AA , respectively.

For the heterostructures, a $6 \times 6 \times 1$ \mathbf{k} -grid is used. The in-plane lattice parameters are fixed to $\sqrt{2}a_{\text{BSO}}$ (a_{BSO} being the bulk BaSnO₃ lattice spacing) (see supplementary figure 1). For the non-periodic systems, vacuum of about 150 \AA is included and a dipole correction is applied in the [001] direction in order to prevent unphysical interactions between neighboring replica. In this case, we fix the first two BaSnO₃ unit cells to the bulk structure to simulate the bulk-like interior of the substrate, and relax the other internal coordinates. For computing the electronic properties, a $20 \times 20 \times 1$ \mathbf{k} -grid is adopted for all systems. This parameter ensures converged densities of states and electron/hole charge densities up to 0.01 e per a^2 . Atomic structures are visualized using the software package VESTA [47].

DATA AVAILABILITY

Input and output files can be downloaded free of charge from the NOMAD Repository [48] at the following link: <https://dx.doi.org/10.17172/NOMAD/2021.03.10-1>.

ACKNOWLEDGMENTS

This work was supported by the project BaStet (Leibniz Senatsausschuss Wettbewerb, No. K74/2017) and was performed in the framework of GraFOX, a Leibniz Science Campus, partially funded by the Leibniz Association. We acknowledge the North-German Supercomputing Alliance (HLRN) for providing HPC resources that have contributed to the research results reported in this paper (project bep00078). W. A. thanks Martin Albrecht, Martina Zupancic, and Toni Markurt (Leibniz-Institut für Kristallzüchtung, Berlin) Dmitrii Nabok, Le Fang, and Sebastian Tillack (Humboldt-Universität zu Berlin) as well as Kookrin Char (Seoul National University) for fruitful discussions.

AUTHOR CONTRIBUTIONS

W.A. performed the atomistic simulations and analyzed the data. All authors discussed the results and wrote the paper.

COMPETING INTERESTS

The authors declare no competing interests.

ADDITIONAL INFORMATION

Supplementary information is available for this paper at (<https://...>).

REFERENCES

-
- [1] Ohtomo, A. & Hwang, H. Y. A high-mobility electron gas at the LaAlO₃/SrTiO₃ heterointerface. *Nature* **427**, 423 (2004).
- [2] Mannhart, J. & Schlom, D. G. Oxide interfaces—an opportunity for electronics. *Science* **327**, 1607–1611 (2010).
- [3] Bert, J. A. et al. Direct imaging of the coexistence of ferromagnetism and superconductivity at the LaAlO₃/SrTiO₃ interface. *Nat. Phys.* **7**, 767 (2011).
- [4] Nakagawa, N., Hwang, H. Y. & Muller, D. A. Why some interfaces cannot be sharp. *Nat. Mater.* **5**, 204 (2006).
- [5] Huijben, M. et al. Structure–property relation of SrTiO₃/LaAlO₃ interfaces. *Adv. Mater.* **21**, 1665–1677 (2009).
- [6] Chambers, S. et al. Instability, intermixing and electronic structure at the epitaxial LaAlO₃/SrTiO₃(001) heterojunction. *Surf. Sci. Rep.* **65**, 317–352 (2010).
- [7] Thiel, S., Hammerl, G., Schmehl, A., Schneider, C. W. & Mannhart, J. Tunable quasi-two-dimensional electron gases in oxide heterostructures. *Science* **313**, 1942–1945 (2006).
- [8] Thiel, S. et al. Electron scattering at dislocations in LaAlO₃/SrTiO₃ interfaces. *Phys. Rev. Lett.* **102**, 046809 (2009).
- [9] Xie, Y., Bell, C., Hikita, Y., Harashima, S. & Hwang, H. Y. Enhancing electron mobility at the LaAlO₃/SrTiO₃ interface by surface control. *Adv. Mater.* **25**, 4735–4738 (2013).
- [10] Cancellieri, C. et al. Polaronic metal state at the LaAlO₃/SrTiO₃ interface. *Nat. Commun.* **7**, 10386 (2016).
- [11] Reinle-Schmitt, M. et al. Tunable conductivity threshold at polar oxide interfaces. *Nat. Commun.* **3**, 932 (2012).
- [12] Pentcheva, R. & Pickett, W. E. Avoiding the polarization catastrophe in LaAlO₃ overlayers on SrTiO₃(001) through polar distortion. *Phys. Rev. Lett.* **102**, 107602 (2009).
- [13] Stengel, M. First-principles modeling of electrostatically doped perovskite systems. *Phys. Rev. Lett.* **106**, 136803 (2011).
- [14] Cantoni, C. et al. Electron transfer and ionic displacements at the origin of the 2D electron gas at the LAO/STO interface: Direct measurements with atomic-column spatial resolution. *Adv. Mater.* **24**, 3952–3957 (2012).
- [15] Gazquez, J. et al. Competition between polar and nonpolar lattice distortions in oxide quantum wells: New critical thickness at polar interfaces. *Phys. Rev. Lett.* **119**, 106102 (2017).
- [16] Kim, H. J. et al. High mobility in a stable transparent perovskite oxide. *Appl. Phys. Express* **5**, 061102 (2012).
- [17] Paudel, T. R. & Tsymbal, E. Y. Prediction of a mobile two-dimensional electron gas at the LaScO₃/BaSnO₃(001) interface. *Phys. Rev. B* **96**, 245423 (2017).
- [18] Wang, Y., Tang, W., Cheng, J., Nazir, S. & Yang, K. High-mobility two-dimensional electron gas in SrGeO₃- and BaSnO₃-based perovskite oxide heterostructures: an ab initio study. *Phys. Chem. Chem. Phys.* **18**, 31924–31929 (2016).
- [19] Krishnaswamy, K. et al. BaSnO₃ as a channel material in perovskite oxide heterostructures. *Appl. Phys. Lett.* **108**, 083501 (2016).
- [20] Kim, U. et al. All-perovskite transparent high mobility field effect using epitaxial BaSnO₃ and LaInO₃. *APL Mater.* **3**, 036101 (2015).
- [21] Lee, W.-J. et al. Transparent perovskite barium stannate with high electron mobility and thermal stability. *Annu. Rev. Mater. Res.* **47**, 391–423 (2017).
- [22] Niedermeier, C. A. et al. Electron effective mass and mobility limits in degenerate perovskite stannate BaSnO₃. *Phys. Rev. B* **95**, 161202 (2017).
- [23] Niedermeier, C. A., Kamiya, T. & Moram, M. A. Polaron coupling constants in BaSnO₃. Preprint at <https://arxiv.org/pdf/1612.01343v1.pdf> (2016).
- [24] Chambers, S. A., Kaspar, T. C., Prakash, A., Haugstad, G. & Jalan, B. Band alignment at epitaxial BaSnO₃/SrTiO₃(001) and BaSnO₃/LaAlO₃(001) heterojunctions. *Appl. Phys. Lett.* **108**, 152104 (2016).
- [25] Kim, Y., Kim, Y. M., Shin, J. & Char, K. LaInO₃/BaSnO₃ polar interface on MgO substrates. *APL Mater.* **6**, 096104 (2018).
- [26] Kim, Y. M. et al. Interface polarization model for a 2-dimensional electron gas at the BaSnO₃/LaInO₃ interface. *Sci. Rep.* **9**, 16202 (2019).
- [27] Zupancic, M. et al. Role of the interface in controlling the epitaxial relationship between orthorhombic LaInO₃ and cubic BaSnO₃. *Phys. Rev. Materials* **4**, 123605 (2020).
- [28] Zupancic, M., Aggoune, W., Draxl, C. & Albrecht, M. Termination at the BaSnO₃ surface and LaInO₃/BaSnO₃ interface. In preparation (2021).
- [29] Lee, H. et al. Direct observation of a two-dimensional hole gas at oxide interfaces. *Nat. Mater.* **17**, 231 (2018).
- [30] Galazka, Z. et al. Melt growth and physical properties of bulk lano3 single crystals. *physica status solidi (a)* **218**, 2100016 (2021).
- [31] See Supplemental Material at <http://link....org/> for computational details as well as for additional information on structural and electronic properties of the pp-type and other selected heterostructures. The Born effective

- charges in pristine systems are computed by Ref. [4].
- [32] Glazer, A. M. The classification of tilted octahedra in perovskites. *Acta Crystallogr., Sect. B* **28**, 3384–3392 (1972).
- [33] Aggoune, W. *et al.* Electronic and optical properties of cubic BaSnO₃: a combined theoretical and experimental study. Preprint at <https://arxiv.org/abs/2105.07817> (2021).
- [34] Aggoune, W. *et al.* Fingerprints of optical absorption in the perovskite LaInO₃: Insight from many-body theory and experiment. *Phys. Rev. B* **103**, 115105 (2021).
- [35] Maznichenko, I. V., Ostanin, S., Ernst, A., Henk, J. & Mertig, I. Formation and tuning of 2D electron gas in perovskite heterostructures. *Phys. Status Solidi B* **257**, 1900540 (2020).
- [36] Millis, A. J. & Schlom, D. G. Electron-hole liquids in transition-metal oxide heterostructures. *Phys. Rev. B* **82**, 073101 (2010).
- [37] Eisenstein, J. & MacDonald, A. Bose–einstein condensation of excitons in bilayer electron systems. *Nature* **432**, 691–694 (2004).
- [38] King-Smith, R. D. & Vanderbilt, D. Theory of polarization of crystalline solids. *Phys. Rev. B* **47**, 1651–1654 (1993).
- [39] Resta, R., Posternak, M. & Baldereschi, A. Towards a quantum theory of polarization in ferroelectrics: The case of KNbO₃. *Phys. Rev. Lett.* **70**, 1010–1013 (1993).
- [40] Jang, D. H. *et al.* Single crystal growth and optical properties of a transparent perovskite oxide LaInO₃. *J. Appl. Phys.* **121**, 125109 (2017).
- [41] Zhou, J.-J. & Bernardi, M. Predicting charge transport in the presence of polarons: The beyond-quasiparticle regime in SrTiO₃. *Phys. Rev. Research* **1**, 033138 (2019).
- [42] Krishnaswamy, K., Himmetoglu, B., Kang, Y., Janotti, A. & Van de Walle, C. G. First-principles analysis of electron transport in BaSnO₃. *Phys. Rev. B* **95**, 205202 (2017).
- [43] Nabok, D., Höffling, B. & Draxl, C. Energy-level alignment at organic/inorganic interfaces from first principles: Example of poly(para-phenylene)/rock-salt ZnO(100). *Chem. Mater.* **31**, 7143–7150 (2019).
- [44] Galazka, Z. *et al.* Melt growth and properties of bulk BaSnO₃ single crystals. *J. Phys. Condens. Matter* **29**, 075701 (2016).
- [45] Perdew, J. P. *et al.* Restoring the density-gradient expansion for exchange in solids and surfaces. *Phys. Rev. Lett.* **100**, 136406 (2008).
- [46] Blum, V. *et al.* Ab initio molecular simulations with numeric atom-centered orbitals. *Comput. Phys. Commun* **180**, 2175 – 2196 (2009).
- [47] Momma, K. & Izumi, F. *VESTA3* for three-dimensional visualization of crystal, volumetric and morphology data. *J. Appl. Cryst.* **44**, 1272–1276 (2011).
- [48] Draxl, C. & Scheffler, M. The nomad laboratory: from data sharing to artificial intelligence. *J. Phys. Mater.* **2**, 036001 (2019).
- [49] Gulans, A. *et al.* exciting: a full-potential all-electron package implementing density-functional theory and many-body perturbation theory. *J. Phys. Condens. Matter.* **26**, 363202 (2014).

Supporting Information on

"Tuning two-dimensional electron (hole) gases at $\text{LaInO}_3/\text{BaSnO}_3$ interfaces: Impact of polar distortions, termination, and thickness"Wahib Aggoune¹ and Claudia Draxl^{1,2}¹*Institut für Physik and IRIS Adlershof, Humboldt-Universität zu Berlin, 12489 Berlin, Germany*²*European Theoretical Spectroscopy Facility (ETSF)*

SUPPLEMENTARY METHODS

Local density of states and charge densities

The local density of states per unit cell (LDOS) in the out-of-plane direction is obtained by summing over the atom-projected density of states of the atoms within the respective unit cell. The density of the two-dimensional electron gas (2DEG) is evaluated by integrating the LDOS of the occupied states between the conduction-band minimum and the Fermi level (E_F) and summing over all planes *i.e.* AO ($A = \text{La}, \text{Ba}$) and BO_2 ($B = \text{Sn}, \text{In}$). Likewise, the hole-gas density (2DHG) is obtained from the corresponding integral over the unoccupied states between the E_F and valence-band maximum. For the non-stoichiometric nn- and pp-type periodic heterostructures, we integrate over the states comprised between the mid gap and the Fermi level.

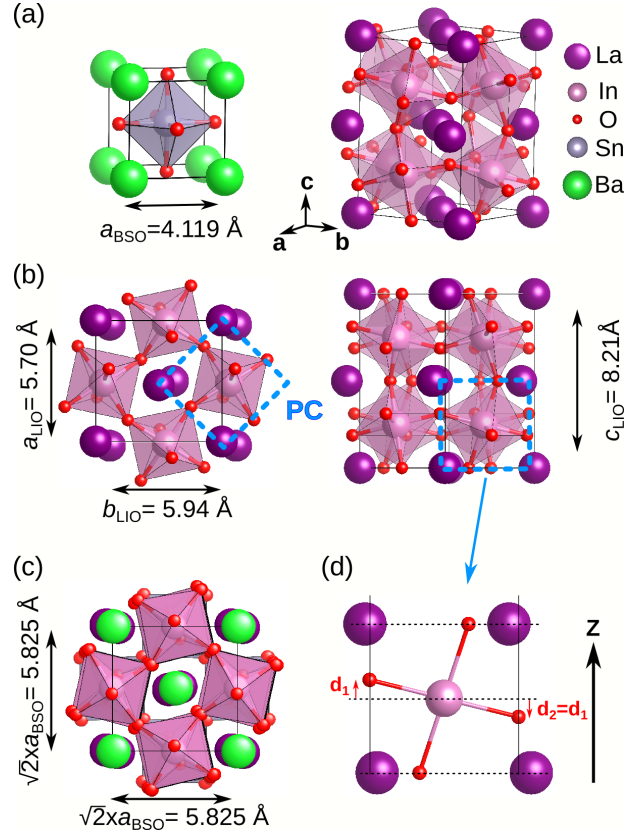
SUPPLEMENTARY DISCUSSION

Structural properties

The primitive unit cell in BaSnO_3 contains 5 atoms, with highly symmetric (non-tilted) SnO_6 octahedra [see Supplementary figure 1(a)]. The pseudocubic LaInO_3 unit cell is defined as the structure exhibiting the same volume per LaInO_3 formula unit as the orthorhombic cell [see Supplementary figure 1(b)]. The calculated averaged pseudocubic lattice parameter is 4.116 Å. In Supplementary figure 1(c) we show the top view of an interface where the in-plane lattice parameters are fixed to $\sqrt{2}a_{\text{BSO}}$ (a_{BSO} being the bulk BaSnO_3 lattice spacing). Details on the structural parameters of the considered heterostructures are summarized in Table Supplementary table 1.

As shown in Supplementary figure 2(a) for the stoichiometric periodic heterostructure $\text{LIO}_{12}/\text{BSO}_{10}$, the out-of-plane lattice spacing increases locally due to the gradual change of the octahedra tilts, amounting to about +3% with respect to that of bulk BaSnO_3 at the interface. This finding is in very good agreement with experimental observations [1], reporting a local increase of about 2%. We also clearly see that 10 unit cells of BaSnO_3 are enough to minimize the interaction with its replica, since the out-of-plane lattice spacing in the middle of BaSnO_3 block is similar to its bulk counterpart [Supplementary figure 2(a)].

Polarization

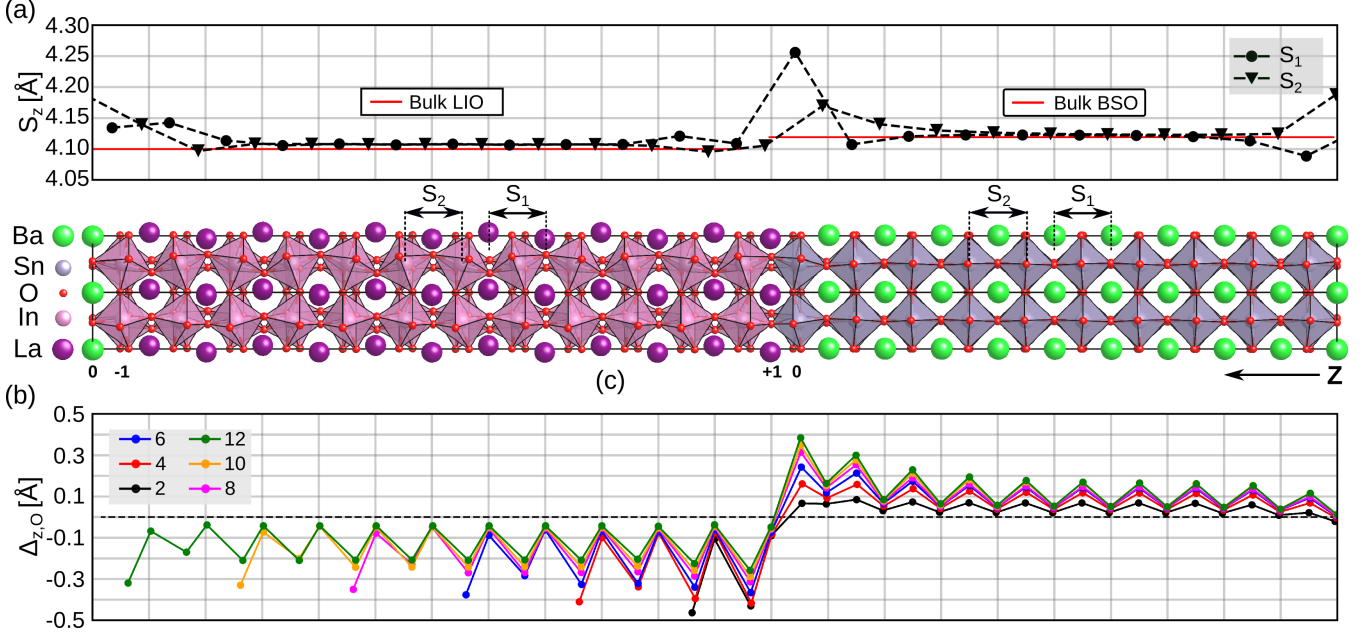


Supplementary figure 1. **Structural properties of pristine materials.** (a) Primitive cell of cubic BaSnO_3 (left) and orthorhombic LaInO_3 (right). (b) Top and side view of the LaInO_3 unit cell. The corresponding pseudocubic unit cell (PC) is highlighted by dashed light-blue lines. (c) Top view of the heterostructure where the in-plane lattice dimensions are fixed to the bulk BaSnO_3 geometry. (d) Equal out-of-plane displacements (with opposite sign) of the inequivalent oxygen atoms with respect to In by tilting the octahedra.

A qualitative trend of the polarization induced by the structural distortions are estimated using the relative atomic displacements in the supercell together with the Born effective charges (Z^*) calculated for bulk BaSnO_3 and LaInO_3 , along the z direction. Such approach has been largely used in literature for the description of polarization effects in oxides interfaces [2]. The fact that it cannot be fully quantitative, is attributed to local dipoles induced in the heterostructures, which do not exist in the bulk, as well as to the possible appearance of a metallic

Supplementary table 1. Structural parameters of the heterostructure geometries shown in Fig. 1 (stoichiometric periodic $\text{LiO}_{12}/\text{BSO}_{10}$), Fig. 2 (non-stoichiometric periodic nn-type $\text{LiO}_{10}/\text{BSO}_{10}$), and Fig. 3 (stoichiometric non-periodic $\text{LiO}_8/\text{BSO}_{11}$), shown in the main text, as well as in Supplementary figure 5 (non-stoichiometric periodic pp-type $\text{LiO}_{10}/\text{BSO}_{10}$). The non-stoichiometric nn- and pp-type systems are symmetric and have overall nonpolar character.

| Superlattices | Formula | Spacegroup | $a=b=\sqrt{2} a_{\text{BSO}}$ [\AA] | c [\AA] |
|--|--|---------------------------|--|----------------------|
| Stoichiometric $\text{LiO}_{12}/\text{BSO}_{10}$ | $\text{Ba}_{20}\text{Sn}_{20}\text{La}_{24}\text{In}_{24}\text{O}_{132}$ | (7) P c | 5.825 | 90.664 |
| nn-type $\text{LiO}_{10}/\text{BSO}_{10}$ | $\text{Ba}_{18}\text{Sn}_{20}\text{La}_{22}\text{In}_{20}\text{O}_{120}$ | (26) P m c 2 ₁ | 5.825 | 82.498 |
| pp-type $\text{LiO}_{10}/\text{BSO}_{10}$ | $\text{Ba}_{22}\text{Sn}_{20}\text{La}_{18}\text{In}_{20}\text{O}_{120}$ | (26) P m c 2 ₁ | 5.825 | 82.449 |
| Interface (with 150 \AA vacuum) | Formula | Spacegroup | $a=b=\sqrt{2} a_{\text{BSO}}$ [\AA] | c [\AA] |
| Stoichiometric $\text{LiO}_8/\text{BSO}_{11}$ | $\text{Ba}_{22}\text{Sn}_{22}\text{La}_{16}\text{In}_{16}\text{O}_{114}$ | (1) P 1 | 5.825 | 226.283 |



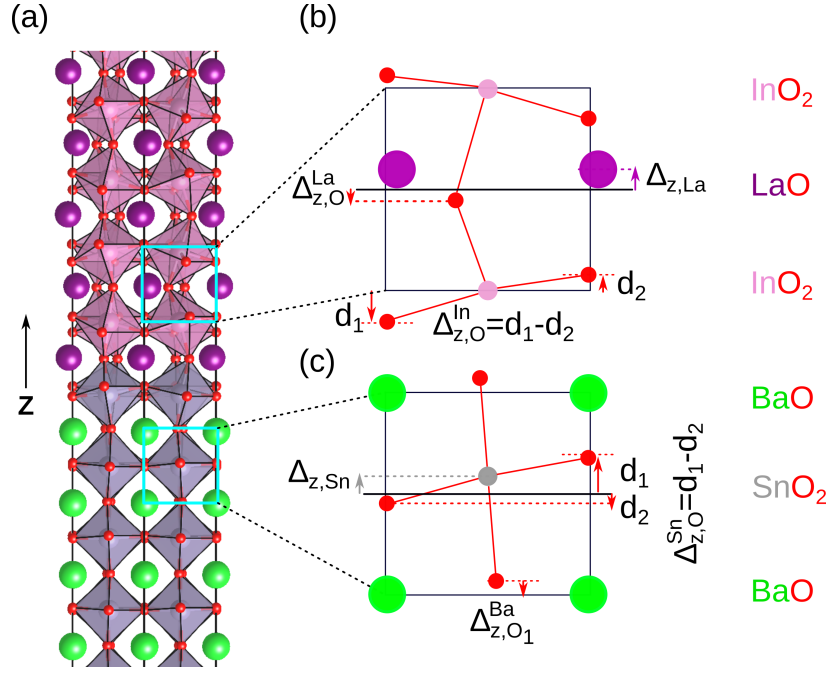
Supplementary figure 2. **Properties of the stoichiometric periodic heterostructure $\text{LiO}_{12}/\text{BSO}_{10}$.** (a) Out-of-plane spacing S_1 (S_2) between adjacent Ba (Sn) atoms within BaSnO_3 and between adjacent La (In) atoms within the LaInO_3 block, also indicated by arrows in the structure model below. The red lines indicate the spacing in the bulk counterparts (b) Oxygen displacements $\Delta_{z,\text{O}}$ within each unit cell for different LaInO_3 thicknesses (in units of the pseudocubic unit cell). The lines are guides to the eye. For details see Supplementary figure 3.

character across the interface. As a consequence, polarization and 2DEG densities are not the same in the two models. However, the periodic heterostructures are nevertheless a valuable approach for analyzing trends, like how the polarization behaves with the thickness of the polar LaInO_3 block.

Z^* are computed within the Berry phase approach [3] using `exciting` [4], an all-electron full-potential code, implementing the family of (L)APW+LO (linearized augmented plane wave plus local orbital) methods. These calculations are performed for the relaxed bulk structures of BaSnO_3 and LaInO_3 (Supplementary figure 1) as obtained by the FHI-aims code, and using the same \mathbf{k} -grid. For the atomic species A (Ba, La), B (Sn, In), and O, muffin-tin radii (R_{MT}) of 2.2, 2.0, and 1.6 bohr are used, respectively. A basis-set cutoff $R_{MT}G_{max}=8$

is adopted, where R_{MT} here refers to the radius of the smallest sphere (1.6 bohr), *i.e.*, $G_{max}=5$.

The results for Ba, Sn, O within the BaO layer, and O within the SnO_2 layer are $Z^*=2.77, 4.44, -3.47,$ and $-1.87,$ respectively. For LaInO_3 , we obtain 3.83, 3.38, $-2.53,$ and $-2.34,$ for La, In, O within the LaO layer, and O within the InO_2 layer, respectively. As depicted in Supplementary figure 1 (d), the InO_2 octahedra in bulk LaInO_3 are tilted, and thus the two inequivalent oxygen atoms are shifted up and down (z direction), respectively, with respect to the In atom by the same amount. Likewise, the inequivalent La atoms within different planes are displaced within the same plane but in opposite direction, away from their centrosymmetric positions. Consequently, the induced polarizations arising from the respective inequivalent atoms cancel each



Supplementary figure 3. **Structural distortions within the stoichiometric periodic heterostructure.** (a) Structural model of LIO₂/BSO₁₀ system. (b) Schematic showing the out-of-plane displacements Δ_z of the different ions within LaInO₃. The unit cell covers the space between adjacent InO₂ planes, taking In as the reference. $\Delta_{z,La}$ and $\Delta_{z,O}^{La}$ represent the displacements from the bulk z coordinate. $\Delta_{z,O}^{In}$ represents the difference between the displacements d_1 and d_2 of the inequivalent O atoms with respect to the cation In. (c) Same as (b) for the ions within BaSnO₃. In this case, the unit cell is defined as the space between adjacent BaO planes, taking Ba as the reference. $\Delta_{z,O}^{Ba}$ represents the distance from its bulk z coordinate. $\Delta_{z,O}^{Sn}$ represents the difference between the displacements d_1 and d_2 of the inequivalent O atoms along z . $\Delta_{z,Sn}$ is the displacement of the Sn atom from its bulk z coordinate.

other in bulk LaInO₃, resulting in zero total polarization [see Supplementary figure 1(d)]. This means that the tilting of octahedra does not necessarily induce a polarization. Such octahedra tilts are thus termed nonpolar distortions [5]. They can, however, induce a polarization in the out-of-plane direction when the oxygen displacements are unequal, *i.e.*, $\Delta_{z,O} = d_1 - d_2 \neq 0$. This situation is indeed observed in our heterostructures [see the example in Supplementary figure 3 and Supplementary figure 6(c)].

Using a simple linear approximation [6], the local polarization per unit cell is written as

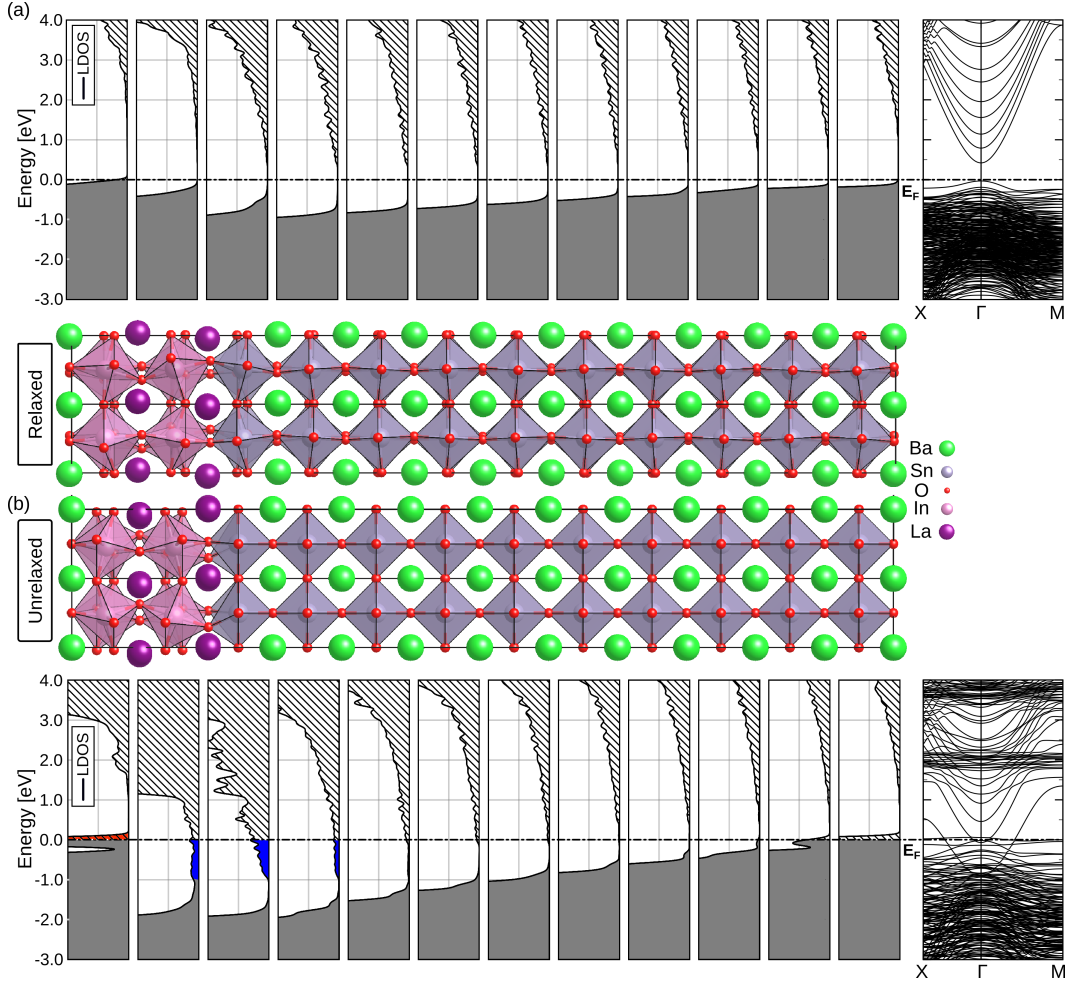
$$P_z = \frac{1}{\Omega} \sum_i Z_{z,i}^* \Delta_{z,i} \quad (1)$$

where, Ω is the volume of the unit cell and $Z_{z,i}^*$ is the Born effective charge of ion i along the z direction. For the choice of unit cells and definitions of the displacements Δ_z of the different ions within LaInO₃ and BaSnO₃ see Supplementary figure 3.

In Supplementary figure 2(b), we display the variation of the oxygen distortions, $\Delta_{z,O}$, along the considered layers for the stoichiometric periodic heterostructures with composition LIO_{*m*}/BSO₁₀ ($m = 2, 4, 6, 8, 10, 12$). As we can see, the O atoms are shifted up (z direction) within

the BaSnO₃ side and down within the LaInO₃ side. As $Z_{z,O}^*$ is negative, the induced polarization in the BaSnO₃ (LaInO₃) side is opposite to (the same as) the out-of-plane direction. In the LaInO₃ side, it counteracts the formal polarization, while in the BaSnO₃ side it leads to a minimization of the polar discontinuity at the interface. The distortions $\Delta_{z,O}$ in the BaSnO₃ side increase with the LaInO₃ thickness, while they decrease in the LaInO₃ side. Note that $\Delta_{z,O}$ has the main contribution to the polar distortions shown in Figs. 1 (c) and (g) of the main text.

The highest value of polarization induced by these distortions is found for the periodic heterostructure LIO₂/BSO₁₀ [see Supplementary figure 4 and Fig. 1(g) in the main text]. Counteracting the formal polarization P_0 , it hampers the electronic charge transfer up to a thickness of 4 pseudocubic LaInO₃ unit cells [Fig. 1(f) in the main text]. Ignoring these distortions by considering *unrelaxed* periodic heterostructure, we find that it has a metallic character with a complete electronic reconstruction [see Supplementary figure 4(b)]. Consequently, a 2DEG of about $0.5 e$ per a^2 is formed as predicted by the polar-catastrophe model that is based on a rigid, unrelaxed lattice. This result emphasizes the critical role of polar distortions in compensating



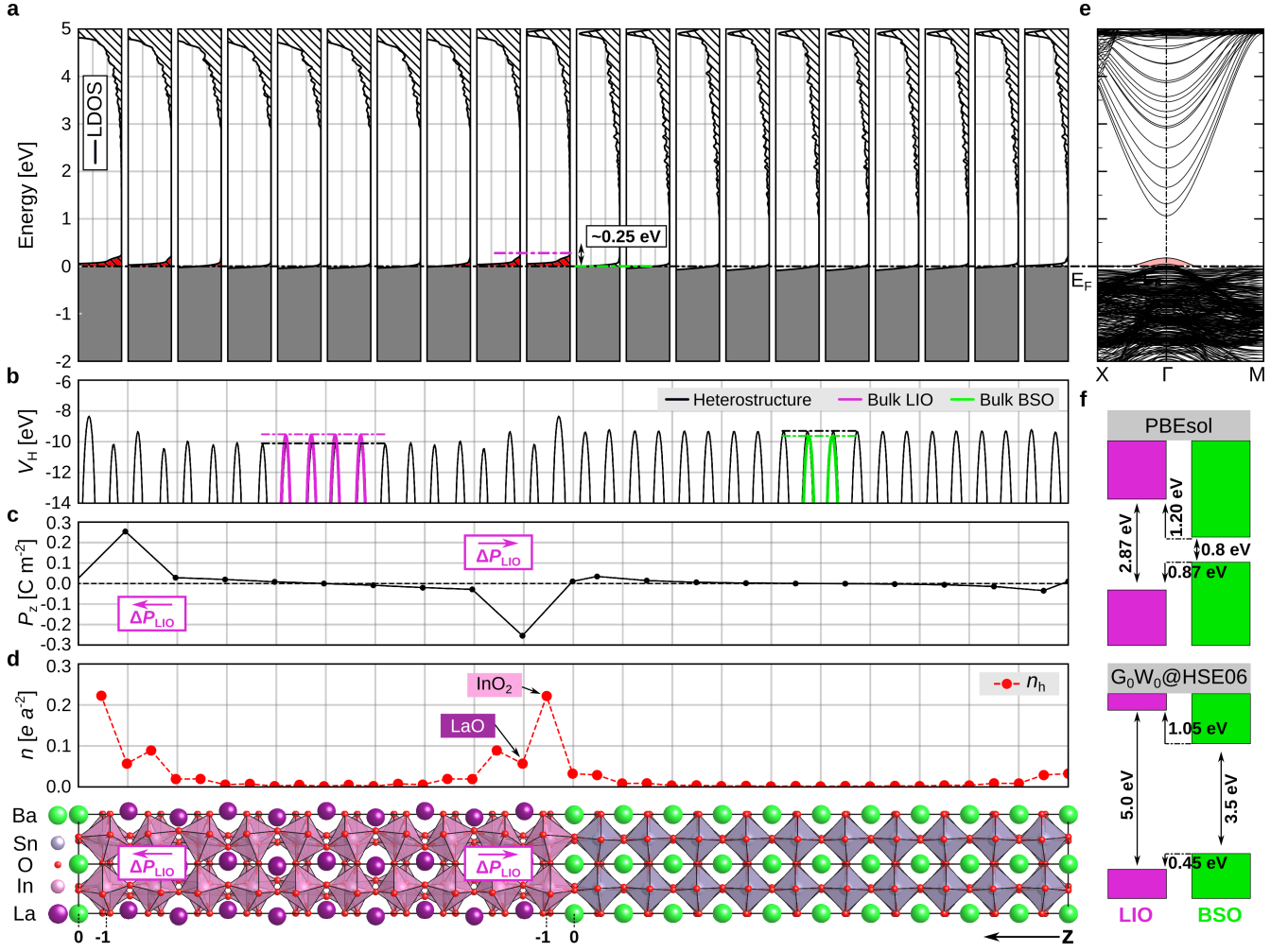
Supplementary figure 4. **Comparison between the *relaxed* (a) and the *unrelaxed* (b) stoichiometric periodic heterostructure $\text{LiO}_2/\text{BSO}_{10}$.** The LDOS (left) and the band structure (right) show the semiconducting character of the former and the metallic character of the latter system.

the polar discontinuity. Reaching the *critical* thickness of 4 pseudocubic LaInO_3 unit cells, a 2DEG forms inside BaSnO_3 . Increasing the LaInO_3 thickness, the charge density increases and the polar distortions decrease. The latter behavior implies that the octahedral tilt within the LaInO_3 converges to that of the bulk counterpart upon increasing the thickness. The same behavior is found for the non-periodic systems, but with less pronounced structural distortions in the BaSnO_3 substrate [see also Fig. 3 (c), (f) and (g) in the main text].

Comparison between n- and p-type interfaces

In Supplementary figure 5, we present the electronic properties of a non-stoichiometric periodic heterostructure, where the LaInO_3 slab terminates with an $(\text{InO}_2)^{-1}$ plane on both sides (termed pp-type). The electronic band structure shows that this system has metallic character, where the (former) valence band in LaInO_3 is partially depleted by one e per a^2 [see Supplementary figure 5(e)]. The effective hole mass is about 1.21

m_e , significantly higher than that of bulk LaInO_3 (0.48 m_e) [7]. The octahedral tilt decreases gradually from the LaInO_3 to the BaSnO_3 side. However, in this case the BaO termination favors nonpolar distortions within the BaSnO_3 side (*i.e.*, equal displacements of the inequivalent O atoms). Consequently, polar distortions appear mainly within the LaInO_3 side, inducing polarizations oriented toward the interface. This local dipole causes an upward shift of the valence-band edge inside LaInO_3 near the interface as also seen in the averaged in-plane electrostatic potential [see Supplementary figure 5(b)]. The valence-band edge at the BaSnO_3 side is almost the same in all unit cells as polar distortions are negligible [see Supplementary figure 5(a) and (c)]. Integrating the LDOS over the partially unoccupied valence states, we find that the 2DHG stays in the LaInO_3 side of the interface and is confined within one pseudocubic unit cell, amounting to 0.5 e per a^2 at each side [see Supplementary figure 5(d)]. It is mainly hosted by O- p states within the InO_2 layers.



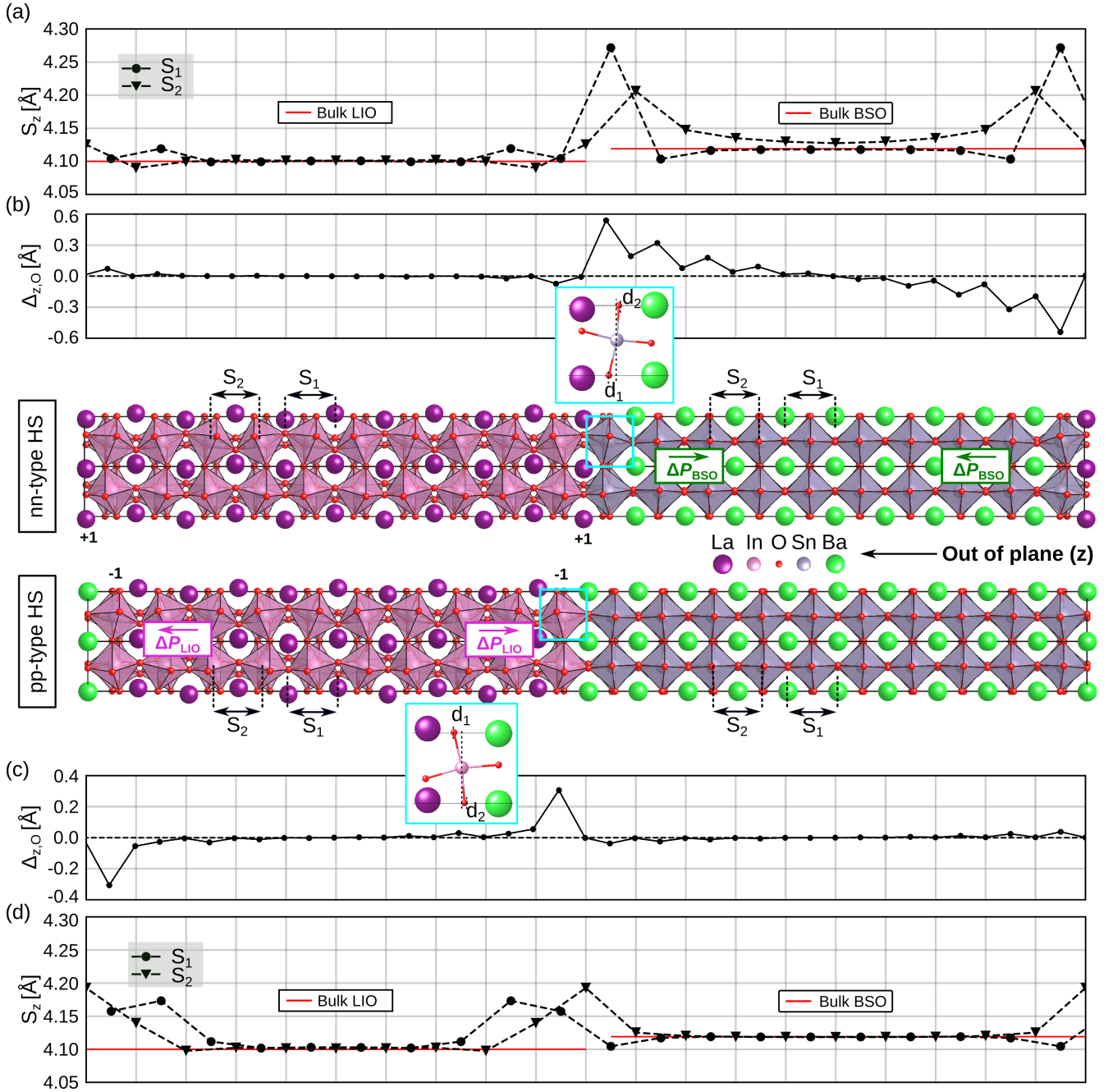
Supplementary figure 5. **Non-stoichiometric pp-type periodic heterostructure:** the system is formed by $\text{LIO}_{10}/\text{BSO}_{10}$ in out-of-plane direction z (bottom), that is shared between panels (a), (b), (c), and (d) as their horizontal axis. The LaInO_3 block is terminated by a $(\text{InO}_2)^{-1}$ plane on both sides. (a) Local density of states per unit cell (LDOS). The Fermi level is set to zero, and the unoccupied states of the (original) valence bands are highlighted by the shaded red area (also in panel (e)). The dashed green and pink lines indicate the alignment of the valence-band edges of BaSnO_3 and LaInO_3 at the interface. (b) In-plane averaged electrostatic potential along the z direction. (c) Total polarization per unit cell. (d) Distribution of the hole charge density obtained by integrating the DOS over the unoccupied valence states indicated by the red color in panel (a). (e) Electronic band structure along X- Γ -M. (f) Band alignment as obtained by using the band gaps of the bulk systems (PBEsol [top] and $G_0W_0@HSE06$ [bottom]), considering the energy difference between the potential of the bulk and the periodic heterostructure as shown in panel (b). The alignment at the interface obtained by PBEsol can be seen in panel (a).

In Supplementary figure 6, we compare the optimized geometries of nn- and pp-type periodic heterostructures. Before analyzing the latter, we note that in a pristine symmetric LaInO_3 slab with InO_2^{-1} termination, the hole charge accumulates on its surfaces, accompanied by structural distortions that tend to screen the discontinuity of the polarization. Combined with BaSnO_3 (pp-type periodic heterostructure), the hole charge stays at the LaInO_3 side. The structural distortions also appear only in the LaInO_3 side [see Supplementary figure 6(b)]. Thus, the interfacial polar discontinuity is less compensated than in the n-type interface, making

the latter more favorable. This explains why, at the interface, (n-type) SnO_2 termination is predominantly found experimentally [8]. This is also confirmed by computing the formation energies, that differ by 0.05 eV per atom (-2.40 eV per atom compared to -2.45 eV per atom).

Band alignment in non-stoichiometric periodic heterostructures

To compute the band offset using the quasiparticle band gaps of the bulk materials BaSnO_3 and LaInO_3 [7, 9], we use an approach based on the electrostatic potential that accounts for all electrostatic



Supplementary figure 6. **Properties of the non-stoichiometric periodic heterostructure.** Out-of-plane spacing S_1 (S_2) between adjacent Ba (Sn) atoms within BaSnO_3 and between adjacent La (In) atoms within the LaInO_3 block, also indicated by arrows in the structure model for the (a) nn-type and (d) pp-type periodic heterostructure. The red lines indicate the spacing in the bulk counterparts. Displacement of oxygen atoms $\Delta_{z,O}$ in the (b) nn-type and (c) pp-type models. For details see Supplementary figure 3.

effects at the interface, *i.e.*, charge rearrangements upon interface formation and interface dipoles [10]. We first estimate the energy shift between the in-plane averaged electrostatic potential of the pristine components (orthorhombic LaInO_3 and cubic BaSnO_3) and that of the periodic heterostructure [see Fig. 2(b) in the main text

and Supplementary figure 5(b)]. This energy difference is used to shift the valence- and conduction-band edges calculated for the bulk materials in order to determine the corresponding band alignment in the heterostructure. We note that this approach provides the alignment only away from the interface as the potential-energy shift

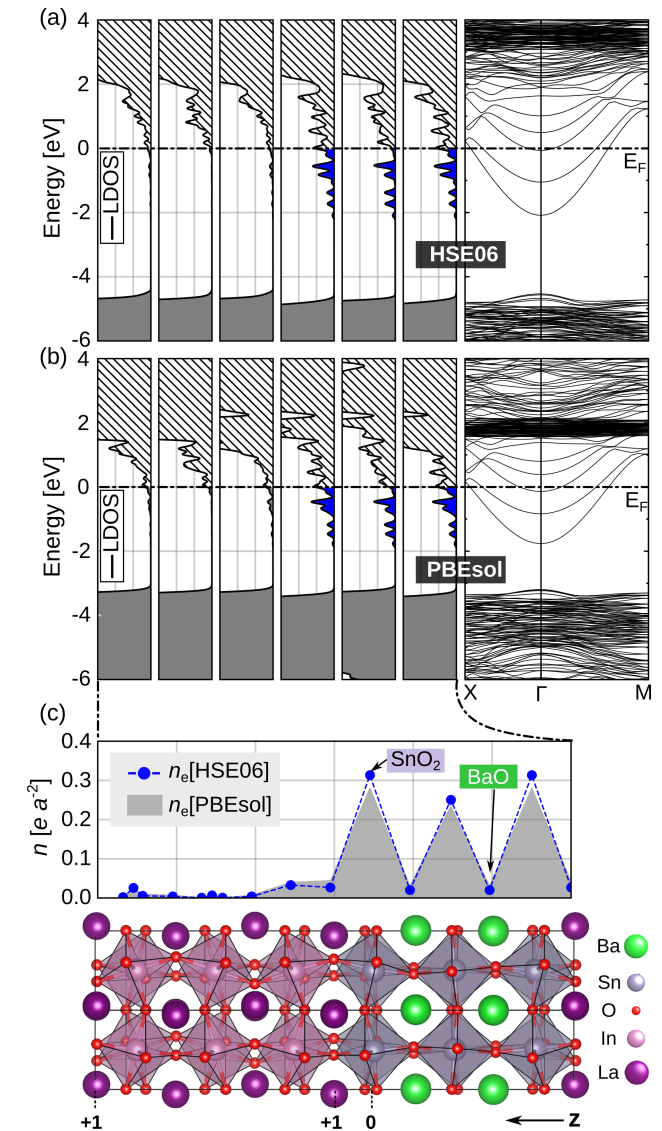
can be only estimated there [see Fig. 2(b) in the main text and Supplementary figure 5(b)]. We find that the conduction-band offset between BaSnO_3 and LaInO_3 is almost the same using the PBEsol gaps or the respective quasiparticle gaps [7, 9] [see Fig. 2(f) in the main text]. Likewise, for the periodic pp-type heterostructure, a similar valence-band offset is found using PBEsol or the quasiparticle gaps [see Supplementary figure 5(f)]. We note that the band alignment exactly at interface can be evaluated from the LDOS only [see Figs. 1(a), 2(a), 3(a) in the main text and Supplementary figure 5(a)]. Overall, these results show that the PBEsol functional is good enough to capture band offset and charge distribution at the interface.

HSE06 calculation for validating the scissor-shift approach

To justify the scissor-shift approach considered above, we compute the electronic properties of a feasible heterostructure using HSE06 for comparison with PBEsol. For more information on its performance for oxide perovskites, we refer to calculations for pristine BaSnO_3 and LaInO_3 materials [7, 9]. In Supplementary figure 7, we depict the results for a non-stoichiometric nn-type periodic heterostructure, formed by three BaSnO_3 unit cells and three pseudocubic LaInO_3 unit cells. Comparing panels (a) and (b), we clearly see that the LDOS obtained by HSE06 and PBEsol, respectively, have similar band alignment and shape within each unit cell. From the right panels, we also see that the band edges are similar. Differences only appear in higher-lying energy bands (between 2 and 4 eV), attributed to the fact that these bands are formed by localized Ba-*d* and -*f* states as well as La-*f* orbitals which are better described by HSE06. Overall, the conduction-band edge is well captured by PBEsol. This can be attributed to the fact that the valence- (conduction-)band edge of both materials is made of delocalized *p*-states (*s*-states). This finding validates the *critical* thickness of 7 pseudocubic LaInO_3 unit cells estimated in the main text for the stoichiometric periodic heterostructure by relying on the offset given by PBEsol [LDOS, Fig. 1(a) in the main text] that is corrected by a scissor shift according to the quasiparticle gaps of the pristine materials [7, 9]. Applying the same procedure, for the non-periodic interface, a *critical* thickness of five pseudocubic LaInO_3 unit cells is found.

Comparison between periodic and non-periodic systems

In the main text, we show that, for a given LaInO_3 thickness, the 2DEG density is higher in the non-periodic heterostructures compared to periodic ones [see Fig. 3(f)]. As shown in Supplementary figure 9 for a thickness of eight pseudocubic LaInO_3 unit cells, the enhanced 2DEG charge density in the non-periodic system is due to the pronounced polar discontinuity at the interface. The latter is attributed to smaller polar distur-



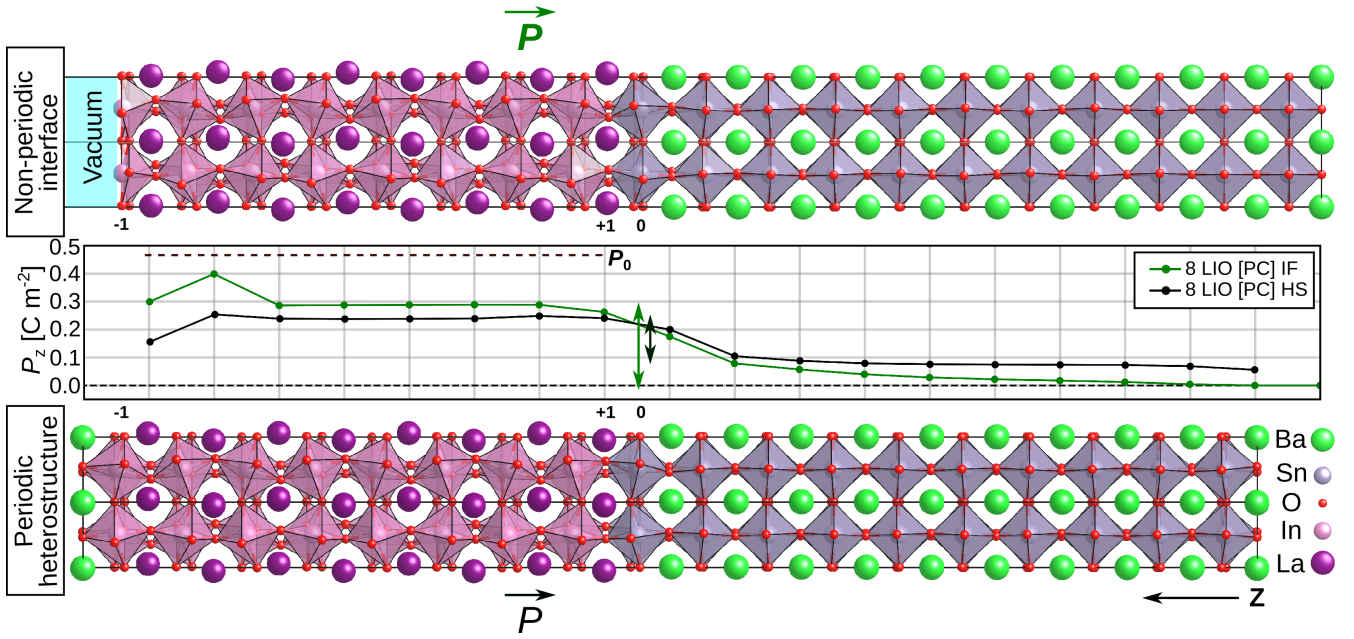
Supplementary figure 7. **Non-stoichiometric periodic nn-type heterostructure:** the system is formed by $\text{LiO}_3/\text{BSO}_3$ in the out-of-plane direction z (bottom), that is shared between panels (a), (b), and (c) as their horizontal axis. Local density of states per unit cell (LDOS) obtained using (a) HSE06 and (b) PBEsol. The Fermi level is set to zero, and the electron population of the (original) conduction bands is shown as shaded blue area. The corresponding band structures along X- Γ -M are shown in the right panels. (c) Distribution of the electron charge density obtained by integration over the occupied conduction states indicated by the blue area in panel (a). The electronic distribution obtained by PBEsol (from panel b) is shown for comparison.

tions within the BaSnO_3 side. This, in turn, allows for an extension of the 2DEG up to five unit cells into the BaSnO_3 substrate. In the periodic heterostructures, the significant polar distortions in the BaSnO_3 side reduce the interfacial polar discontinuity and thus the electronic charge density. However, such distortions lead to a con-

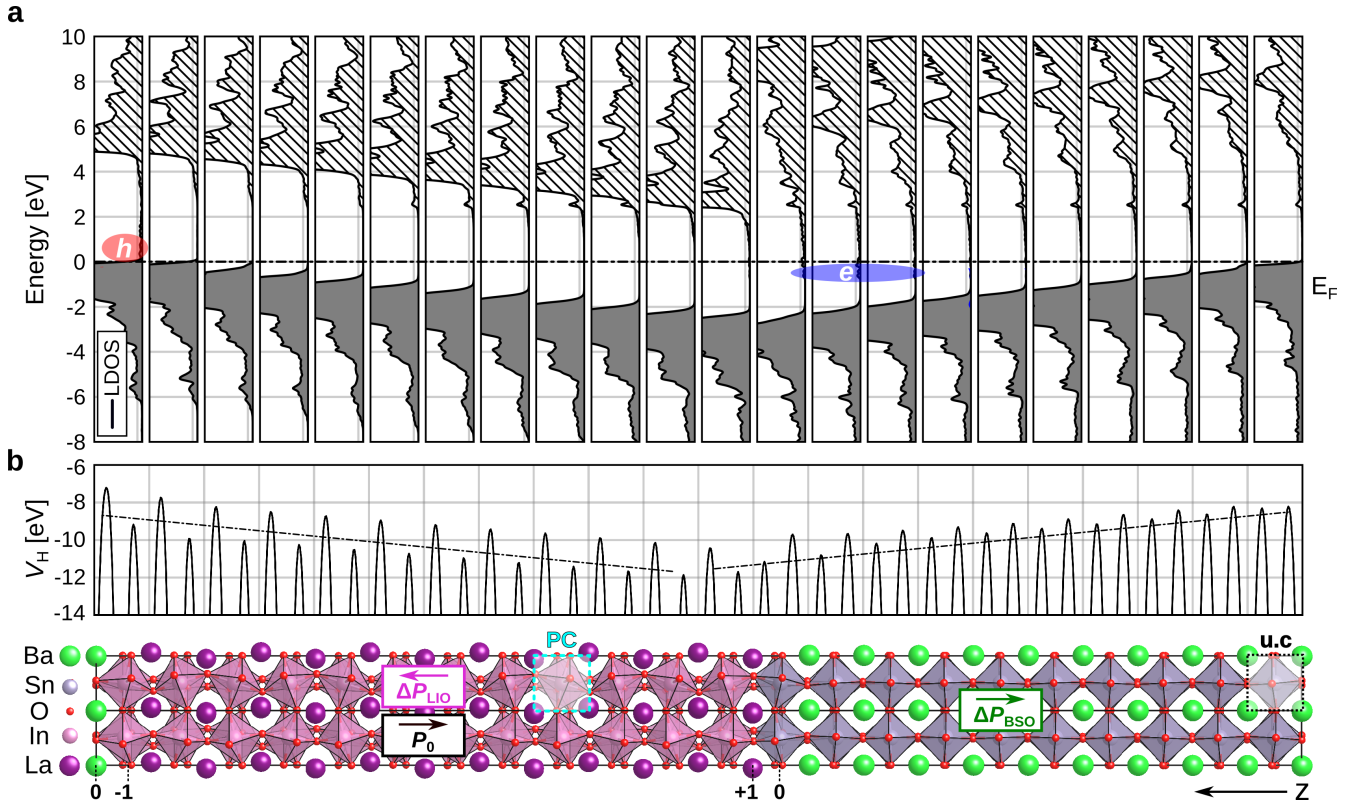
finement of the 2DEG within three BaSnO₃ unit cells compared to five in the non-periodic structure.

SUPPLEMENTARY REFERENCES

- [1] Kim, Y. M. *et al.* Interface polarization model for a 2-dimensional electron gas at the BaSnO₃/LaInO₃ interface. *Sci. Rep.* **9**, 16202 (2019).
- [2] Pentcheva, R. & Pickett, W. E. Avoiding the polarization catastrophe in LaAlO₃ overlayers on SrTiO₃(001) through polar distortion. *Phys. Rev. Lett.* **102**, 107602 (2009).
- [3] King-Smith, R. D. & Vanderbilt, D. Theory of polarization of crystalline solids. *Phys. Rev. B* **47**, 1651–1654 (1993).
- [4] Gulans, A. *et al.* exciting: a full-potential all-electron package implementing density-functional theory and many-body perturbation theory. *J. Phys. Condens. Matter.* **26**, 363202 (2014).
- [5] Gazquez, J. *et al.* Competition between polar and nonpolar lattice distortions in oxide quantum wells: New critical thickness at polar interfaces. *Phys. Rev. Lett.* **119**, 106102 (2017).
- [6] Resta, R., Posternak, M. & Baldereschi, A. Towards a quantum theory of polarization in ferroelectrics: The case of KNbO₃. *Phys. Rev. Lett.* **70**, 1010–1013 (1993).
- [7] Aggoune, W. *et al.* Fingerprints of optical absorption in the perovskite LaInO₃: Insight from many-body theory and experiment. *Phys. Rev. B* **103**, 115105 (2021).
- [8] Zupancic, M., Aggoune, W., Draxl, C. & Albrecht, M. Termination at the BaSnO₃ surface and LaInO₃/BaSnO₃ interface. *In preparation* (2021).
- [9] Aggoune, W. *et al.* Electronic and optical properties of cubic BaSnO₃: a combined theoretical and experimental study. Preprint at <https://arxiv.org/abs/2105.07817> (2021).
- [10] Nabok, D., Höffling, B. & Draxl, C. Energy-level alignment at organic/inorganic interfaces from first principles: Example of poly(para-phenylene)/rock-salt ZnO(100). *Chem. Mater.* **31**, 7143–7150 (2019).



Supplementary figure 8. **Comparison between the polar discontinuity** in the stoichiometric, periodic (termed HS) and non-periodic (termed IF) heterostructures both comprising eight pseudocubic LaInO_3 unit cells. Total polarization in the out-of-plane direction for the non-periodic (green) and periodic (black) heterostructure. The dashed black line indicates the formal polarization P_0 . The vertical arrows highlight the interfacial polar discontinuity.



Supplementary figure 9. (a) Local density of states per unit cell (LDOS) of the stoichiometric periodic $\text{LIO}_{12}/\text{BSO}_{10}$ heterostructure showing higher energy range compared with Fig. 1 in the main text, in order to provide a complete trend of the valence and conduction band. (b) In-plane averaged electrostatic potential along the z direction. The dashed lines are guides to the eye, highlighting the trend of the potential.